BAT-5-9160-1

INTERIM PROGRESS REPORT

on

AN ADVANCED THERMOELECTRIC COMPONENT DEVELOPMENT PROGRAM

to

NATIONAL AERONAUTICS AND SPACE ADMINISTRATION
GODDARD SPACE FLIGHT CENTER

September 17, 1965

W. E. Kortier, Program Director

BATTELLE MEMORIAL INSTITUTE
505 King Avenue
Columbus, Ohio 43201

TABLE OF CONTENTS

TABLE OF CONTENTS
(Continued)

LIST OF TABLES

LIST OF FIGURES

LIST OF FIGURES
(Continued)

LIST OF FIGURES
(Continued)

AN ADVANCED THERMOELECTRIC COMPONENT DEVELOPMENT PROGRAM

ABSTRACT

15592

The tasks represented under this program are intrinsically separated by their diverse technologies and are reported herein as separate chapters. Under Task I, Computer Program Modification, a new program based upon the extension and generalization of an existing program has been written, debugged, and operated. The program in its present form is capable of analyzing thermoelectric generators for space use where the design under investigation uses the static heat transfer mode and geometries based upon right-cylindrical configurations. A rapid means of analysis, which can treat large numbers of cases in order to identify minimum weight designs, is now available as a fundamental tool in lieu of time-consuming and repetitive manual computations. The work performed under Task II, High-Temperature Segmented Thermoelectric Development, has progressed to the point where several schemes are proposed for element fabrication. These schemes are based upon fundamental studies of thermoelectric-materials properties, transition-member bonding between SiGe and PbTe materials, hot-shoe bonding to GeSi material, and PbTe-segment fabrication using an iron-tin shoe alloy material with an expansion coefficient midway between iron and PbTe. Under Task III, Development of a Thermal Insulation and Support Structure, bonding-process optimization has been completed. Specimens composed of multilayered webs and foil and representing variances in web and foil thickness and web spacing have been fabricated. An indication of the surface emittance of the finished insulation structures was obtained by measuring the surfaces of a selected Hastelloy C coupon.

author

INTRODUCTION

This is the Interim Progress Report issued under Contract NAS5-9160 by Battelle Memorial Institute for National Aeronautics and Space Administration, Goddard Space Flight Center. Work under this program was initiated April 6, 1965. The program is made up of three tasks.

	Task	Description
Task I.	Computer Program Modification	Modification of an existing machine code by extension and generalization
Task II.	High-Temperature Segmented Thermoelectric Development	Development work leading to a demonstration of the feasibility of segmenting GeSi and PbTe materials
Task III.	Development of a Thermal Insulation and Support Structure	Fabrication, thermal testing, and structural testing over a broad range of structure designs to obtain empirical design data

The ensuing chapters are identified by task and have been prepared by P. E. Eggers (Task I), J. J. Mueller (Task II), and J. Ketchman and R. W. Wittman (Task III).

TASK I. COMPUTER PROGRAM MODIFICATION

Objective

The objective of this work is to modify an existing thermoelectric digital-computer program for the analysis of thermoelectric generators to achieve:

(1) A generalized program in which the design parameters will be located in the input-data section of the code

(2) An extended program in which subroutines will be added to establish a more complete analysis of the thermal balance, dimensions, and weight of the thermoelectric generator

(3) A detailed program which will trade off total generator weight with thermoelectric dimensions, end-insulation and radial-insulation thickness, and generator length.

Scope of Work

The program was expanded to include the treatment of all known phases of thermoelectric-generator analysis. This included enumeration of the major- and minor-component dimensions and weights, thermal losses through the media surrounding the heat source, and a detailed balance of heat losses with fuel inventory. In addition, the flexibility of the program was extended to include the analysis of several fuel-form arrays, several heat-source-support methods, and thermoelectric arrays. Options have been included in the program to trade off the end-insulation thickness, thermoelectric-element length, and generator length with the total generator weight. An input instruction can be given to the program to (1) print out all calculated data; (2) print out only the total generator weight and a limited number of pertinent generator dimensions (i.e., generator length, end-insulation thickness, element length, and thermoelectric array); and (3) operate a minimum-seeking iterative loop which identifies and prints out data for only the minimum-weight generator.

Formulation of Analytical Model

An analytical model was formulated emphasizing a general case for the design layout of thermoelectric generators. The model is limited to the static-heat-transfer concept and geometries built upon right-cylindrical configurations. The model contains the major and minor weight-contributing components of the generator in a preselected geometric configuration. The major weight-contributing components are:

(1) Fuel form
(2) Fuel-form cladding and liner
(3) Thermoelectrics
(4) Generator case and the radiator fins.

The minor weight-contributing components include:

(1) Insulation

(2) Heat-source support

(3) Thermoelectric associated hardware (peripheral material, interelement insulation, cold- and hot-junction hardware)

(4) Ablator.

Using a parametric approach to generator analysis, the design conditions governing the above-mentioned components can be varied over a range of values yielding minimum-weight combination(s). Sketches (two views) representing the geometric configuration of the model are shown in Figure 1. The nomenclature used for identification of the components is given in the Glossary of Computer Program Terms, Appendix A, Part I.

The fixed conditions of the analytical model are that the fuel form must conform to one of three geometries:

(1) Right-cylinder geometry for single fuel form

(2) Right-cylinder geometry for fuel pins and overall right-cylinder geometry for a fuel block with the locus of all fuel-pin centers being a circle

(3) Right-cylinder geometry for fuel pins in an overall right-cylinder geometry for fuel block with close packing of fuel pins.

These fuel-form arrays are illustrated in Figure 2. Also, the radiator-fin length is constrained to match the generator length (this length excludes the optional ablative thickness on the generator shell).

Development of Computer Program

Based upon the analytical model, the computer program logic provides for the acceptance of input data, the computations, and the handling of output data. The program has been generalized by writing all design parameters into the input data section.

Program Inputs

The program inputs are listed in the Glossary of Computer Program Terms appearing in Appendix A, Part I, and include the following categories:

(1) Material properties of all components (density, thermal conductivity, power density, thermoelectric parameters, modulus of elasticity, emissivity, toughness parameter)

(2) Generator power output (e)

(3) Radiator-fin length, thickness, and weight parameters corresponding to the number of fins selected

(4) Range of generator lengths

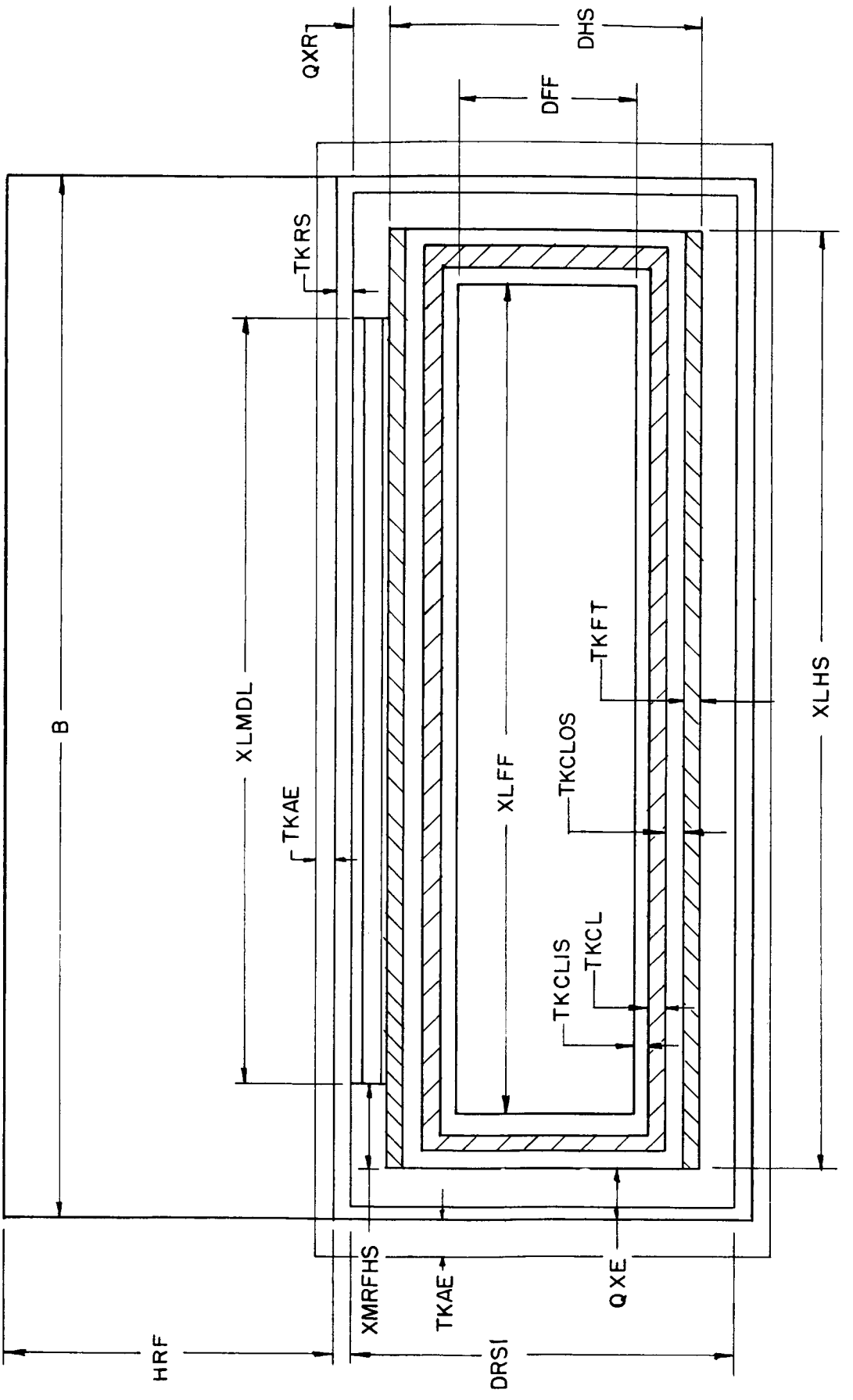

a. Side View

FIGURE 1. ANALYTICAL MODEL

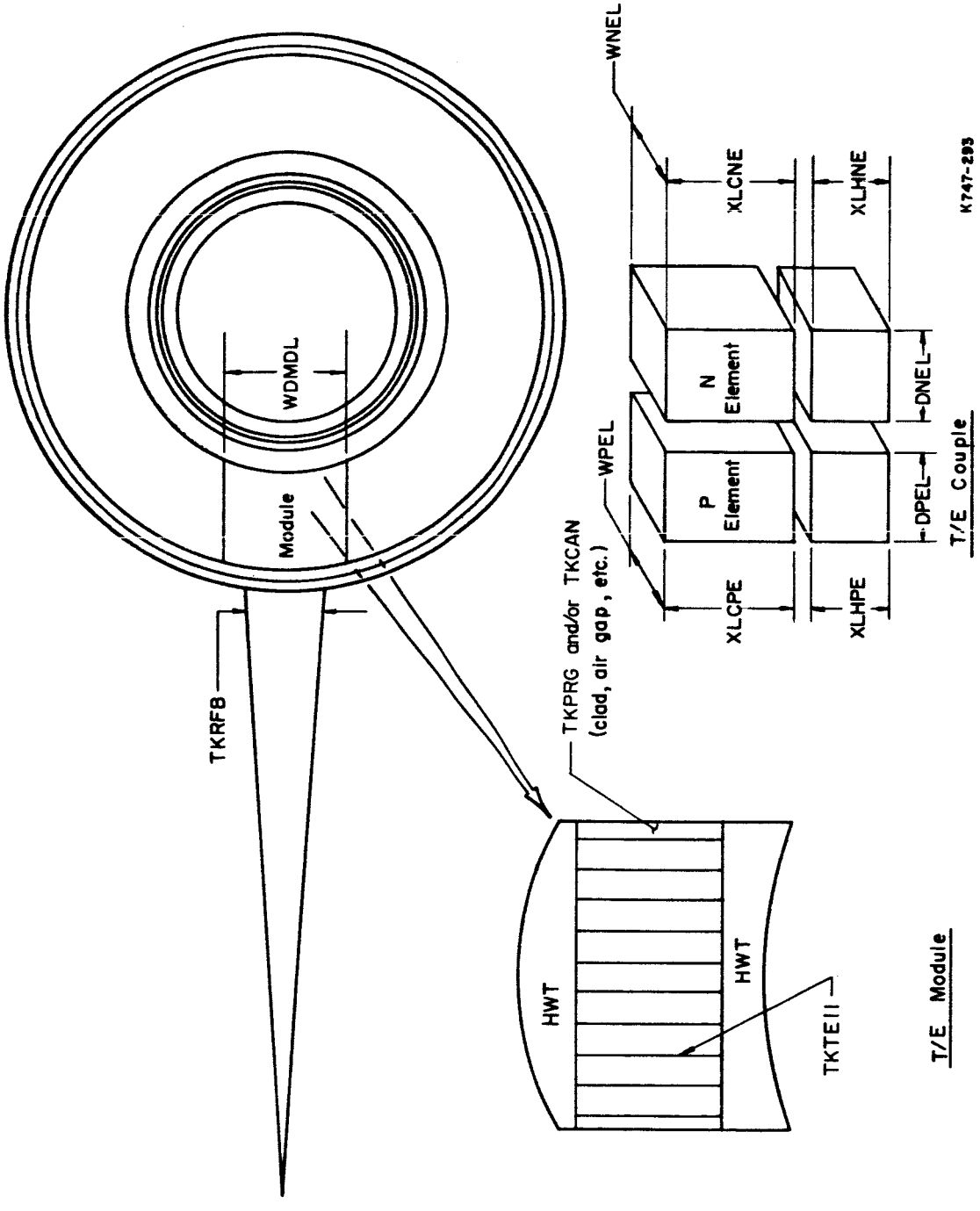

FIGURE 1. (CONTINUED)

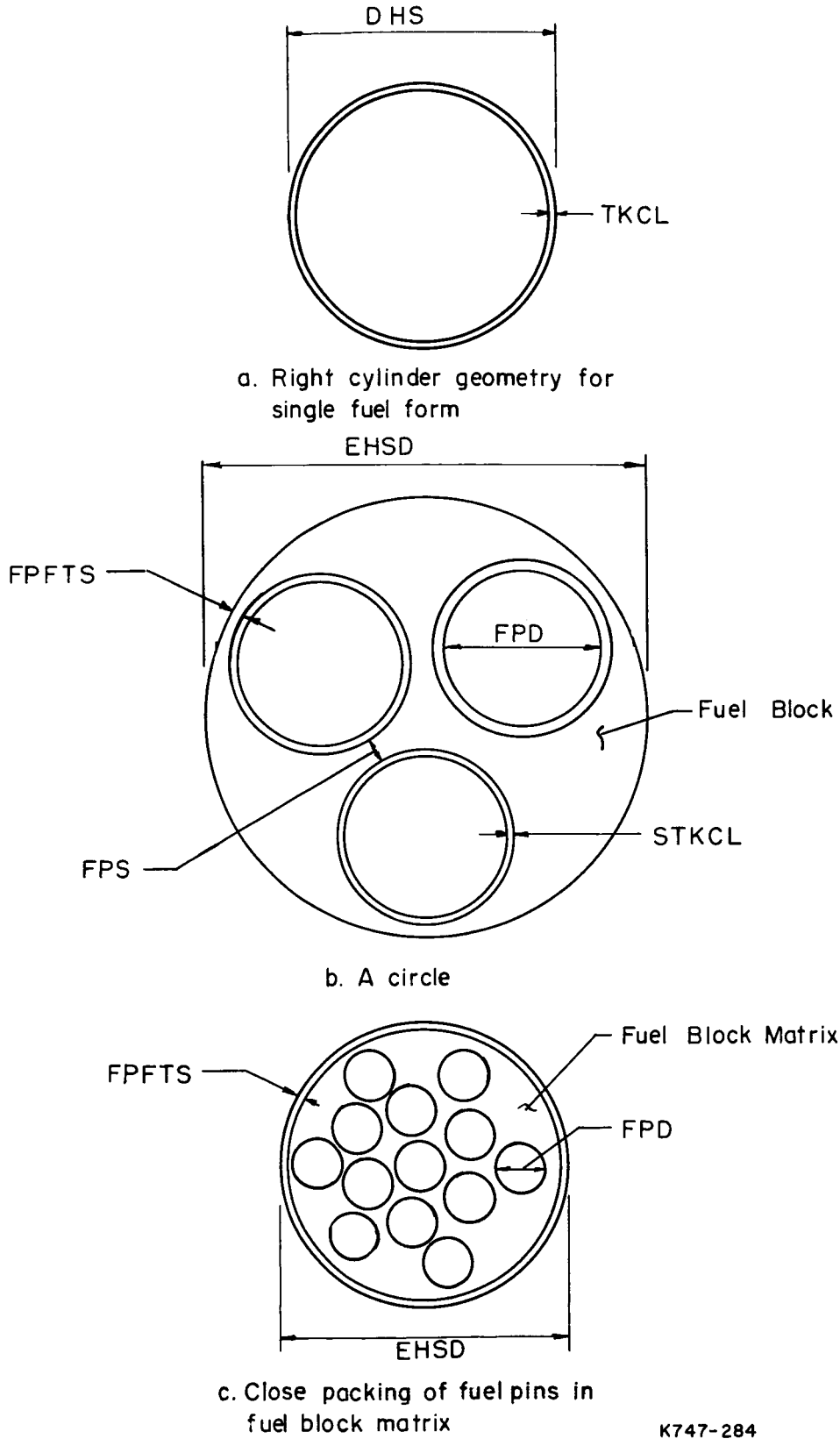

a. Right cylinder geometry for single fuel form

b. A circle

c. Close packing of fuel pins in fuel block matrix

FIGURE 2. FUEL-FORM-ARRAY OPTIONS

(5) Thickness of optional inner and outer claddings, ablator, fuel tube, module periphery, thermoelectric shoes, interelement electrical insulation, generator shell, radiation gap, thermoelectric hardware, end and radial insulation, end and radial heat-source support

(6) Thermoelectric current, L/A ratio, and element segments

(7) Number of modules

(8) Limiting aspect ratios of fuel form, generator casing, and generator envelope

(9) Heat-transfer mode (conductive or radiative)

(10) Temperature profile of generator

(11) Percent of total heat-dump capability of generator ends

(12) Tolerable deflection of heat source based on compression and shear modulus of heat-source support

(13) "g" loading axially and radially

(14) Impact velocity of heat source (cladding analysis)

(15) Epsilon (tolerance) and delta (iterative steps) functions

(16) Maximum number of allowed iterations specified for each subroutine

(17) Optional choice of thermoelectric array (the option to have thermoelectrics, in module form, limited either by heat-source length or heat-source width, or have couples individually dispersed in a matrix and surrounded insulation)

(18) Generator computation sequence (the option to use fixed iterative steps between a minimum and maximum value of generator length, or to use large iterative steps until the minimum weight point is exceeded and to use small iterative steps to locate accurately the minimum weight point)

(19) Thermoelectric-element length computation option (the option to iterate upon element length and print out after each iteration, to print out only after the minimum-weight generator has been reached, or to fix the element length)

(20) Fuel-form array (the option to select for analysis one of three available fuel-form arrays, outlined in the section Formulation of the Analytical Model

(21) Heat-source support option (the option to effect support by the ends of the heat source only, by the radial portion of the heat source only, or by both the ends and the radial portion)

(22) End insulation computation option (the option to iterate upon end-insulation thickness and print out after each iteration, to print out only after the minimum-weight generator has been reached, or to fix the end-insulation thickness).

The optional analyses described in Items (17) through (22) above can be used by iterating on component dimensions and evaluating their effect on the total generator weight. For example, if the thermoelectric-element length is iterated upon, the total area of the thermoelectric module changes in addition to the radial-insulation thickness which follows the element length. Indirectly, the variation of the element length changes the radial bearing area available for heat-source support and also the surface-power-density requirements, total generator-shell dimensions, and weight of the

thermoelectrics. In a similar fashion, the program is capable of iterating upon the end-insulation thickness, total generator length, and thermoelectric-element array to investigate their effect upon the other components of the generator and the total generator weight.

An iteration control has been included in the program to economize on computer operation time. This control mechanism adjusts the size of the iterative steps (delta functions) and tolerance values (epsilon functions) to avoid excessive loss of computer time as a result of inappropriately selected values of these functions. The iteration control will monitor the number of iterations performed, known as the iteration index number, and will terminate the analysis and print out a diagnostic if an adjustment fails to produce a solution within a prescribed recurrence limit.

Program Computations

The computational scheme of the computer code is illustrated in Figure 3 and is itemized in subroutines below. The majority of the subroutine computations are straightforward. However, those that involve more sophisticated treatment have been referenced.

(1) Thermal-Input and -Output Analysis

Calculate: Heat required

Heat dump.

(2) Fuel-Form Analysis

Calculate: Fuel-form volume

Fuel-form weight

Fuel-form dimensions

Number of fuel pins.

(3) Segmenting Subroutine

Maintain fuel form within limiting aspect ratio

Calculate: Number of fuel-form segments.

(4) Cladding Analysis[1]

Calculate: Thickness of cladding

Weight of cladding

Thickness and weight of inner and outer claddings.

(1) Analysis is based on mass required to absorb energy of impact. The development of this analysis appears in NASA Contract NAS5-3697 Final Report.

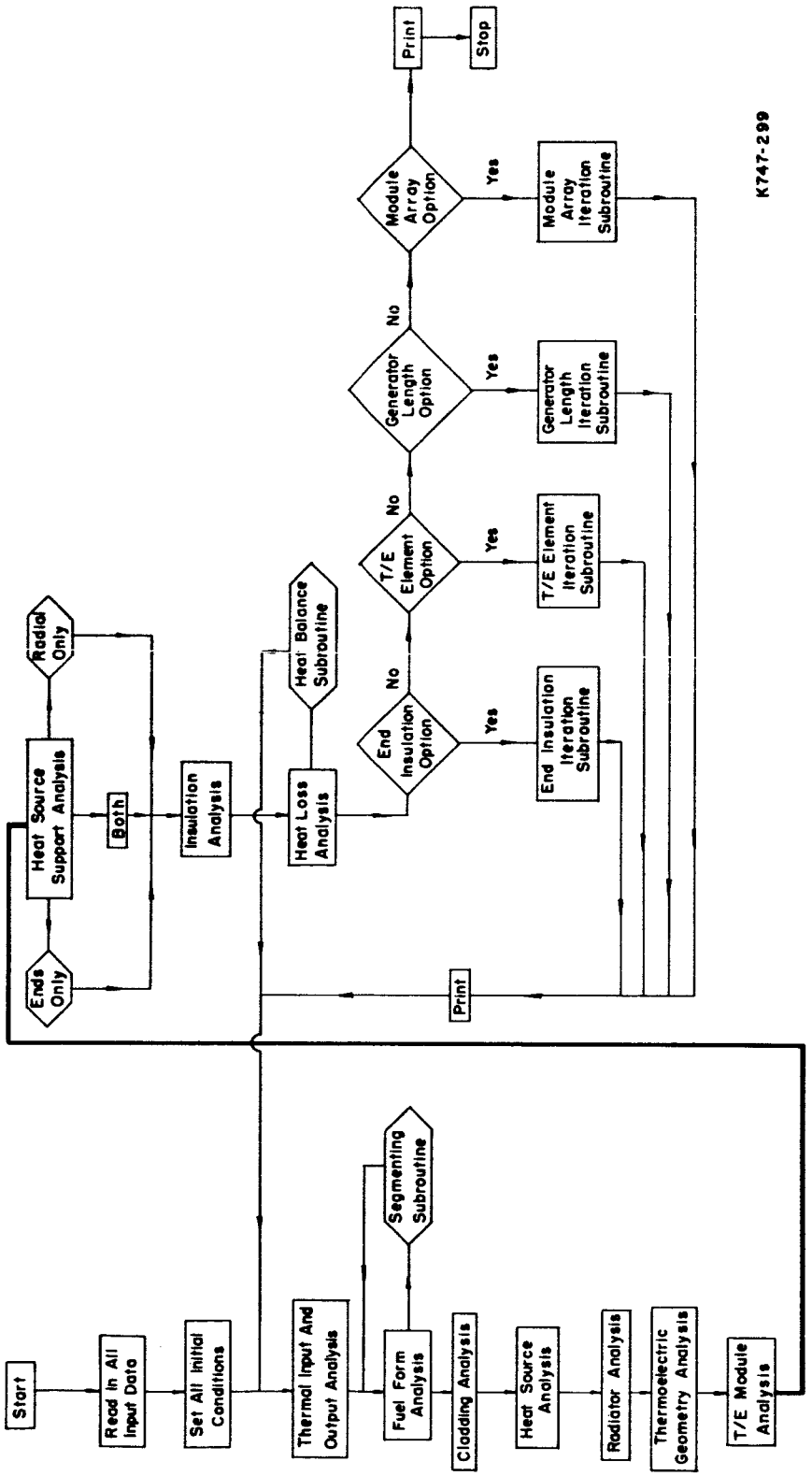

FIGURE 3. COMPUTER CODE FLOW CHART

(5) Heat-Source Analysis

Calculate: Heat-source length
Heat-source diameter
Heat-source volume
Heat-source surface area (available for T/E coverage)
Fuel-block weight.

(6) Radiator Analysis[2]

Calculate: Radiator-fin height
Radiator-fin thickness (base)
Generator-shell diameter (inside)
Generator-shell weight
Radiator-fin weight.

(7) Thermoelectric Geometry Analysis

Calculate: Number of couples
Number of elements
Number of couples per module
N-element dimensions
P-element dimensions.

(8) Thermoelectric-Module-Array Analysis

Calculate: Module width
Module length
Module depth
Heat-loss area for module periphery
Module weight
Weight of module periphery
Thermoelectric weight
Surface power-density required.

(2) This analysis is developed in the Final Report of NASA Contract NAS5-3697, page 25.

(9) Heat-Source-Support Analysis and Subroutine*

Calculate: Area required for transverse support
Area required for longitudinal support
Weight of heat-source support (radially)
Weight of heat-source support (ends)
Deflection of support under given conditions (ends)
Deflection of support under given conditions (radially).

(10) Insulation Analysis

Calculate: Area available for radial insulation
Area available for end insulation
Weight of insulation (ends)
Weight of insulation (radially).

(11) Heat-Loss Analysis

Calculate: Heat loss through electrical and thermal insulation
Heat loss through module periphery
Heat loss through radial insulation(3)
Heat loss through end insulation(3)
Heat loss through radial heat-source support(3)
Effective surface power density available for module
Total heat loss.

(12) Heat-Balance Subroutine

Calculate: Engineering efficiency.

(13) End-Insulation Subroutine

Iterate on end-insulation thickness
Calculate: All output data.

(14) Thermoelectric-Element Subroutine

Iterate on element length
Calculate: All output data.

(15) Generator-Length Subroutine

Iterate on generator length
Calculate: All output data.

*See Appendix B.

(3) This analysis is discussed in the Final Report of NASA Contract NAS5-3697, page 40.

Outputs

The output data listed in the Glossary of Computer Program Terms (Appendix A, Part I) contain the following categories:

(1) Dimensions
(2) Weights
(3) Thermal losses
(4) Iteration index numbers.

The output data may be handled in several ways:

(1) Print out all calculated data for each generator case considered

(2) Print out only the data associated with the minimum weight generator

(3) Plot data directly onto an X-Y plotter by means of array storage of the pertinent data, thus eliminating the time required for manual manipulation of data.

The speed of modern computers permits the analysis of about one case per second with 110 bits of output information per case.

Operation Manual

A manual for the operation of the program entitled "The Space Generator Computer Program Operation Manual" has been written and appears in Appendix A. The manual includes:

(1) Glossary of Computer Program Terms (Appendix A, Part I)

This is a lexicon of the input and output computer language, containing both the definition and the physical units of the terms.

(2) Input Data Form (Appendix A, Part II)

This is a list of program inputs. Several of the inputs are referenced and further discussed in the Input Data Reference section of the form to aid in the data compilation.

(3) Appendix of Recommended Inputs (Appendix A, Part III)

This list contains suggested epsilon and delta functions for use as a starting point in a particular program. These inputs have been estimated on the basis of trial cases of 50-watt(e) and 150-watt(e) generators.

(4) Glossary of Diagnostics (Appendix A, Part IV)

This list contains the corrective measures that are printed out in the event of either an incorrect tolerance or iterative step function. The print-out is in the literal form shown.

Summary

The space-generator computer program has been written and debugged and is now operating. The program provides a versatile and comprehensive analysis tool for the evaluation of space generators characterized by the static-heat-transfer operational mode and geometries of right-cylindrical configuration. The computations performed by the program have been extended to include the minor components of the generator and the energy balance of the device. Thus, the analysis performed by the code closely approximates a real generator design. A rapid means of space-generator analysis, which can treat large numbers of cases in order to identify minimum-weight designs, is now available as a fundamental tool in lieu of time-consuming and repetitive manual computations.

TASK II. HIGH-TEMPERATURE SEGMENTED THERMOELECTRIC DEVELOPMENT

Objective

The overall objective of the thermoelectric development work is to demonstrate the feasibility of segmenting PbTe and SiGe materials. It is the goal of this work to demonstrate that a segmented couple operating between a hot-junction temperature of 1200 K (~ 1700 F) and a cold-junction temperature of 300 K (~ 25 F), will perform at a conversion efficiency of 10 percent or greater without significant degradation.

Scope of Work

The electrical properties of the thermoelectric materials were determined as a function of temperature to provide the data for design calculation of segment lengths and couple performance. Techniques for fabrication of a transition member between SiGe and PbTe, which have widely differing expansion rates, were studied. Tungsten was selected as the contacting member for the SiGe segment on the basis of its proven state-of-the-art usage. Iron was selected for the hot-end contacting member of the lead telluride on the basis of its generally exclusive usage and accepted chemical compatibility. A study of bonding SiGe to a tungsten shoe was initiated for the purpose of establishing a method of producing a bond which is compatible with the sequence and parameters of the overall element-fabrication process. The fabrication of the PbTe segment, although based on state-of-the-art technology, was studied to determine the relative effects of selected hot-isostatic-pressing conditions on the general structural characteristics and PbTe-to-iron shoe bonds. A recently developed iron-base alloy (designated BMI-8) with an expansion rate intermediate between that of iron and PbTe was used as a shoe material for comparative evaluation in this program. The information generated from the supporting studies, which considered separately the different parts of the segmented element, was used to establish schemes for element-fabrication methods and element configuration. An n-type element was fabricated by one of the schemes.

Thermoelectric-Materials Characterization

The Seebeck coefficient and resistivity were determined as a function of temperature for lead telluride (PbTe) consolidated at two temperatures of interest and silicon germanium (SiGe) in its initially purchased, cast form. The data obtained provide the design curves for analytical determination of the segment lengths and the theoretical performance of the overall segmented PbTe-SiGe couple. The thermal conductivities will be obtained from published data.

The apparatus utilized to obtain property measurements, details of test specimen fabrication, and results of the property measurements are discussed below.

Elevated-Temperature Seebeck-Coefficient Test Apparatus

The Seebeck coefficient, which is the rate of change of Seebeck voltage with temperature, is one of the main parameters used to characterize thermoelectric materials. The units generally measured and those used in this work are microvolts per degree centigrade. The Seebeck coefficient was determined as a function of temperature over the appropriate temperature range of operation for each material tested. The equipment used in making these measurements is shown schematically in Figure 4. Figure 5 shows the test apparatus which holds the thermoelement during testing.

To make the Seebeck-coefficient determination, the test element is fitted snugly between two spring-loaded electrodes which are held in guided Lavite insulating blocks. Each contact electrode contains a centrally located sheathed thermocouple which extends from the end of the electrode and supports the specimen at the thermocouple bead. The springs for providing the pressure contact are located at the cold end of the apparatus. The apparatus is slipped into a Vycor tube located in a tube furnace. The specimen is positioned in the center of the furnace and the tube is purged with argon. The heater attached to one of the contacting electrodes is powered to obtain a desired temperature difference across the length of the element (30 C minimum was found to be most reliable). The temperature difference is read by taking separate readings at either end of the specimen. After an initial room-temperature reading is taken, the tube furnace is powered and the temperature slowly increased. The two specimen temperatures and the output voltage of the specimen are plotted as a function of time by means of a temperature (or millivolt) recorder. The curves obtained by joining the respective points are used to obtain the temperature difference and corresponding output voltage at selected points in time.

Elevated-Temperature-Resistivity Test Apparatus

The apparatus used for measuring resistivity as a function of temperature is similar in design to the Seebeck coefficient apparatus, the major exception being that an electrode heater is not used and only one thermocouple is used to measure temperature. The electrical system is shown schematically in Figure 6. The electrodes which support the specimen in the resistivity apparatus are used to carry current which is passed through the specimen. The apparatus incorporates a voltage-probe collar assembly which is fitted over the specimen before it is inserted between the electrodes. This probe collar and its electrical leads are shown in Figure 7.

The probe collar consists of two circular rings, each of which contain three equally spaced, radially positioned probe screws. The rings are fastened parallel to one another at a fixed distance by insulating spacers. The specimen is positioned centrally in the collars and is held firmly by the six probe screws. The electrical leads attached to the collars are used to measure the average voltage drop between the two sets of probe screws.

During operation, a 100-cycle alternating current of approximately 0.7 ampere is passed through the specimen and measured on a 1-ampere-range precision meter. The voltage drop between the probes is measured with a Ballantine a-c vacuum-tube voltmeter. Current and voltage readings are taken as the temperature of the specimen is increased gradually from room temperatures to the maximum desired temperature.

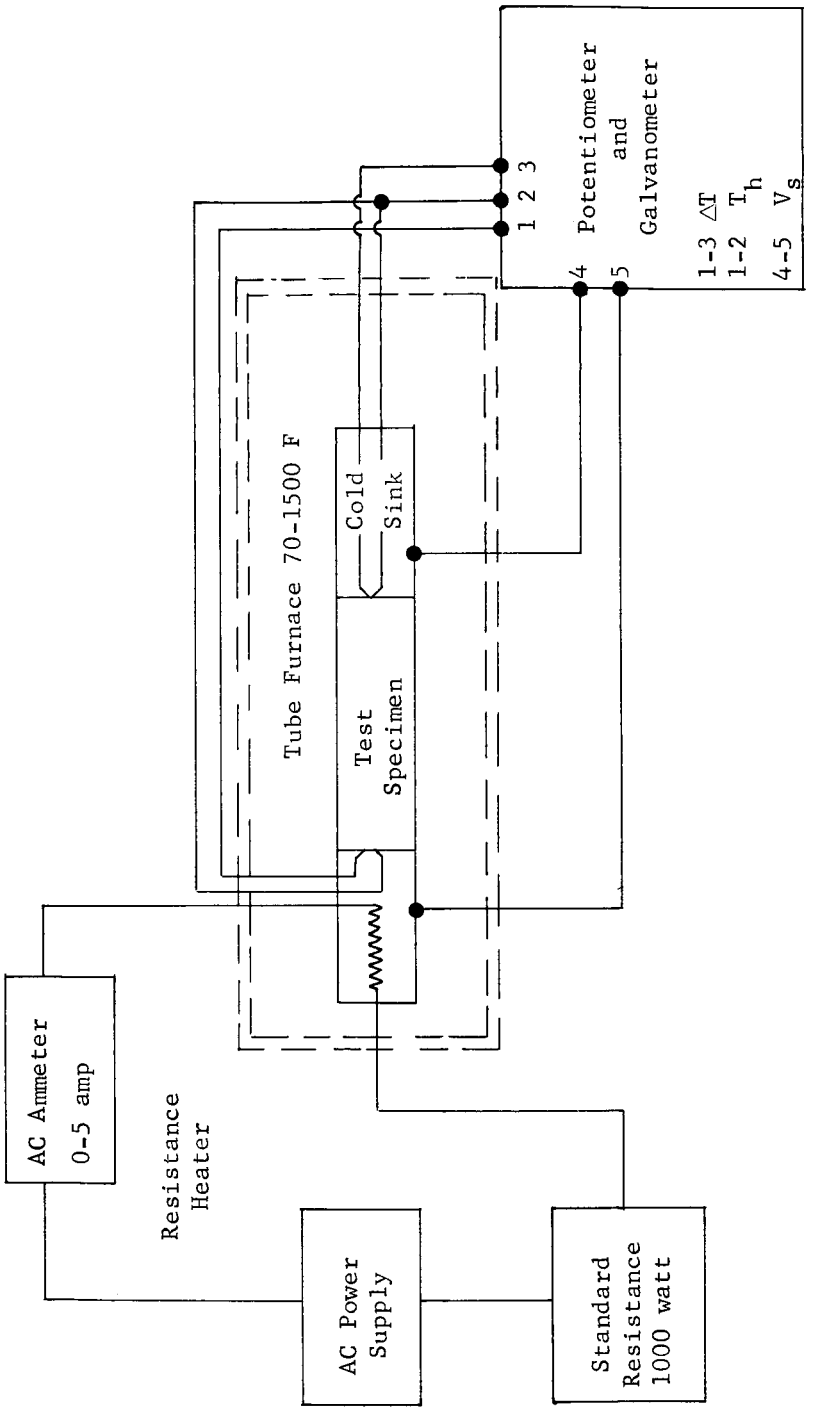

FIGURE 4. SCHEMATIC FOR ELEVATED-TEMPERATURE SEEBECK-COEFFICIENT-MEASURING APPARATUS

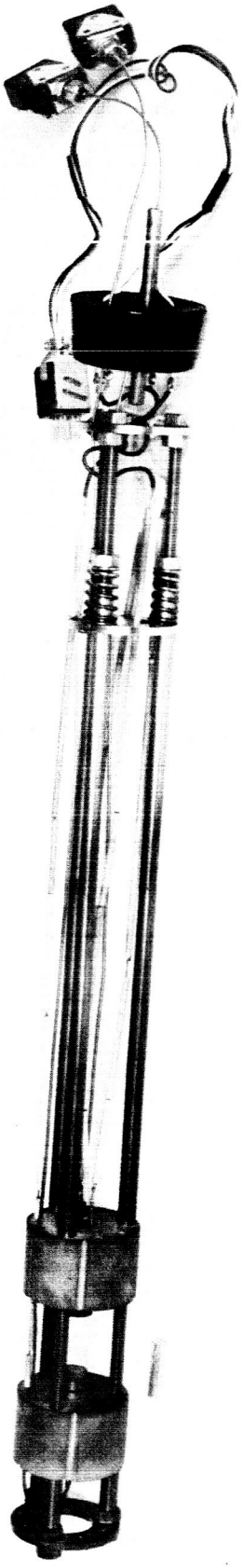

18803

FIGURE 5. DEVICE FOR MEASURING SEEBECK COEFFICIENT

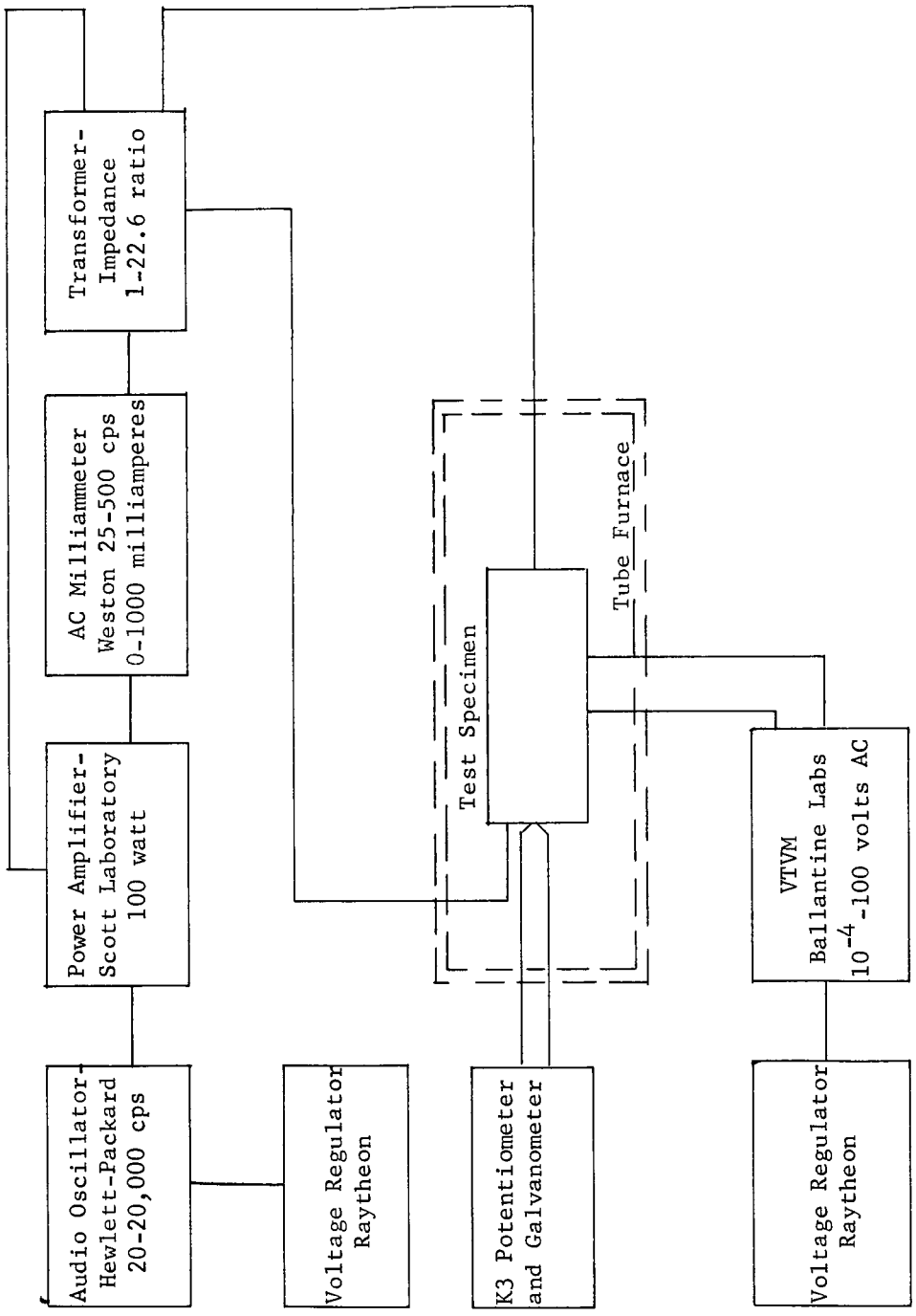

FIGURE 6. SCHEMATIC FOR ELEVATED-TEMPERATURE-RESISTIVITY MEASURING APPARATUS

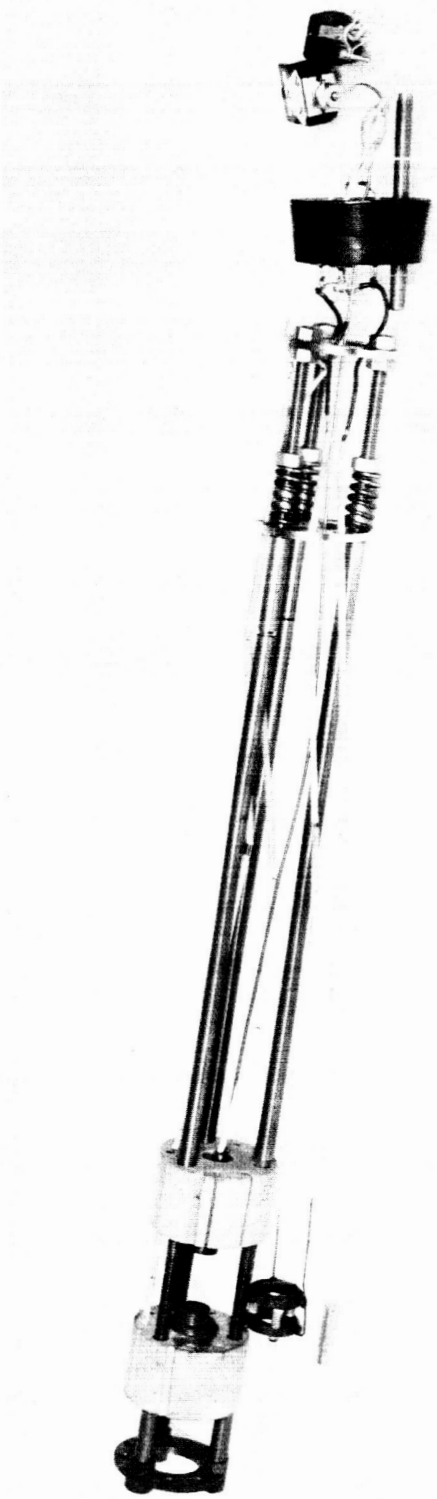

18801

FIGURE 7. DEVICE FOR MEASURING ELEVATED-TEMPERATURE RESISTIVITY

Heating is performed with the apparatus contained in an argon-filled Vycor tube positioned in a tube furnace.

The resistivity is calculated, using the relationship $\rho = R\frac{A}{L} = \frac{VA}{IL}$, where ρ is the resistivity in ohm-cm, V is the measured voltage drop, I is the measured current (in amperes) passed through the specimen, L is the distance in centimeters over which the voltage drop is determined (distance between probe collars), and A is the area of the specimen cross section in square centimeters. The values obtained are plotted as a function of the temperature at which the readings were taken.

Specimen Preparation and Test Results

Lead Telluride. The hot-isostatic-pressing process was selected for the fabrication of the PbTe-Fe composite of the segmented element. Consequently, the specimens used for electrical-property measurements were processed in this manner. The basis for the selection of the hot-isostatic process is discussed in a later section of the report.

The lead telluride was purchased in powder form from Minnesota Mining and Manufacturing Company. Three formulations of lead telluride were used, conforming to the standard designations Tegs 2p, Tegs 2n, and Tegs 3p. The Tegs 3p-PbTe was considered a supplement to the other two types and was selected because of its reportedly greater durability over Tegs 2p-PbTe. This characteristic could make it a potential replacement for the Tegs 2p-type material.

Test-Specimen Preparation

The specimens for electrical-property measurements were prepared from minus 100-mesh powder according to the following procedure.

(1) The powder was loaded into a tubular rubber mold, evacuated, and then hydrostatically pressed at room temperature to produce a rodlike green body approximately 1/4 inch in diameter.

(2) The green-pressed PbTe was encased in a mica sleeve and an outer, tubular, stainless steel container. Mica has been found to be satisfactory encasing material having no effect on the electrical properties.

(3) The canned specimen was sealed in an electron-beam welder, resulting in a vacuum within the can.

(4) The canned specimen was consolidated further by hot-isostatic pressing for 1 hour at 2500 psi. Two hot-isostatic-pressing temperatures were selected to represent the higher and lower pressing temperatures considered applicable for PbTe-SiGe segmenting. The two temperatures were 1200 F and 900 F.

(5) The specimens were decanned as the final step in their fabrication.

Test Results. The Seebeck coefficient and resistivity curves resulting from the tests are presented in Appendix C. All three PbTe materials fabricated at 1200 F were characterized, while the Tegs 3p PbTe fabricated at 900 F was excluded from characterization. The much lower power-producing capability (based on power-factor calculation of the specimen pressed at 1200 F) and the observed poor shoe-bonding characteristic of the Tegs 3p material provided the basis for subsequent exclusion of this material from the study.

The average properties of each material are listed in Table 1. The averages were determined over the operating range of 150 C to 500 C. The Seebeck coefficients, resistivities, and calculated power factors are compared. Lead telluride elements of the pressed and sintered type which were purchased from 3M Company were used for reference purposes. Their measured electrical properties are included in Table 1 for comparison.

The power factors for both the Tegs 2p- and 2n-type PbTe specimens pressed at 1200 F were greater than those for the reference elements. The differences are mainly attributable to the higher Seebeck coefficients of the materials pressed at 1200 F. The power factors for both the p- and n-type specimens pressed at 900 F are lower than those for the reference elements. The lower values result from a lower Seebeck coefficient for the n-type PbTe and a higher resistivity for the p-type PbTe. Since the power factors for the Tegs 2-type PbTe pressed at 900 and 1200 F were greater than 90 percent of the power factors for the reference elements, the properties were accepted for couple calculations. The pressing temperature used will depend on the results of the couple-fabrication development.

The power factor for the hot-pressed Tegs 3p PbTe compared favorably with that for the reference elements. However, the values were so much lower than the Tegs 2p PbTe values that further consideration of the Tegs 3p PbTe was questioned. The poor results obtained in attempts to join this material to iron by an established technique strengthened the decision to tentatively exclude the Tegs 3p PbTe from further study.

Silicon Germanium. Silicon germanium was purchased from Radio Corporation of America (RCA) in raw ingot form. The 1/4-inch-diameter specimens for property measurements were obtained by abrasive cutting and grinding. No difficulties were encountered in this operation.

The properties were measured and the data compared with the data supplied by RCA for the specific materials purchased. The average values of Seebeck coefficient and resistivity calculated between 500 and 900 C were compared. The average values of resistivity differed by less than 10 percent, as is apparent from the data shown below.

	Average Resistivity of SiGe (500-900 C), μohm-cm	
	n-Type	p-Type
RCA Data	2.89	1.98
Battelle Measurements	3.04	1.89

TABLE 1. ELECTRICAL PROPERTIES OF PbTe ELEMENTS

Average Values Between 150 and 500 C

Type of Element	Seebeck Coefficient, μv/C	Resistivity, μohm-cm	Power Factor (S^2/ρ), $10^{-6}\left(\frac{V}{C}\right)^2$/ohm-cm
Elements Hot Isostatically Pressed at 1200 F			
Tegs 2p	247	4175	14.6
Tegs 2n	258	3750	17.8
Tegs 3p	125	2650	5.9
Elements Hot Isostatically Pressed at 900 F			
Tegs 2p	261	5975	11.4
Tegs 2n	235	3920	14.1
3M Elements Measured by Battelle			
Tegs 2p	225	4175	12.1
Tegs 2n	248	4030	15.3
Tegs 3p	137	2990	6.4

BATTELLE MEMORIAL INSTITUTE

Difficulties were encountered, however, in obtaining reproducible values of Seebeck coefficient. The variability in test results appeared to be the result of random variations in the thermal conduction at the thermocouple contacts. The problem was minimized considerably when the specimen length was reduced to about 1/2 inch. Data were then obtained which matched the RCA data over most of the temperature range. At the upper temperatures, however, the Battelle data tended to deviate, sometimes at abnormal rates, indicating error in the measurement.

On the basis of the indicated correspondence of Seebeck-coefficient values over the lower range of temperatures and the good correspondence of the resistivity values over the entire range, the RCA data were selected for use in couple calculations. The electrical-property curves for the SiGe materials are given in Appendix C. The average values of the Seebeck coefficients over the temperature range 500 to 900 C are given below.

	Average Seebeck Coefficient of SiGe (500-900 C), μv/C	
	n-Type	p-Type
RCA Data	290	234

Transition-Member Bonding

The greatly differing thermal-expansion rates of SiGe and PbTe [~2 and ~10 μin./(in.)(F), respectively] dictate the need for an intermediate transition member to accomplish joining of these two thermoelectric-element segments. On the basis of the state-of-the-art technology, tungsten can be joined to SiGe, and iron (powder product) to PbTe, for service as shoes. The problem of joining SiGe and PbTe segments thus reduces to one of joining tungsten to iron within the limitations of processing of the two thermoelectric materials and achieving bonds to their respective shoe materials. The maximum temperature for processing PbTe is in the vicinity of 1500 F, at which point PbTe becomes very plastic. The SiGe-W bonds formed by a direct reaction process are limited to operating temperatures below about 1000 F. If exceeded, continued reaction with tungsten occurs which results in cracking of the SiGe. This is assumed to be the result of the reaction product having a specific volume widely differing from that of its makeup constituents.

The aim in this study is to explore several bonding combinations to arrive at one which is compatible with a potential element fabrication schedule. The use of temperatures higher than 1000 F was predicated on schemes which involve either, (1) reacting the tungsten and SiGe after forming the transition member or, (2) using a braze-bonded SiGe tungsten-composite which might withstand the high temperatures of subsequent pressure bonding to the transition member.

Figure 8 shows two basic approaches considered for joining iron and tungsten to form the transition member. Nickel is used as a solid state bonding agent in both cases. The combination shown in Type A of Figure 8 incorporates an alloy layer (Therlo) with an expansion rate between those of the iron and tungsten members (2.5 vs 3.3 vs 6.3/F). Although this combination of constituents provides a more gradual transition in expansion rate than that shown in Type B of Figure 8, the latter was found to be

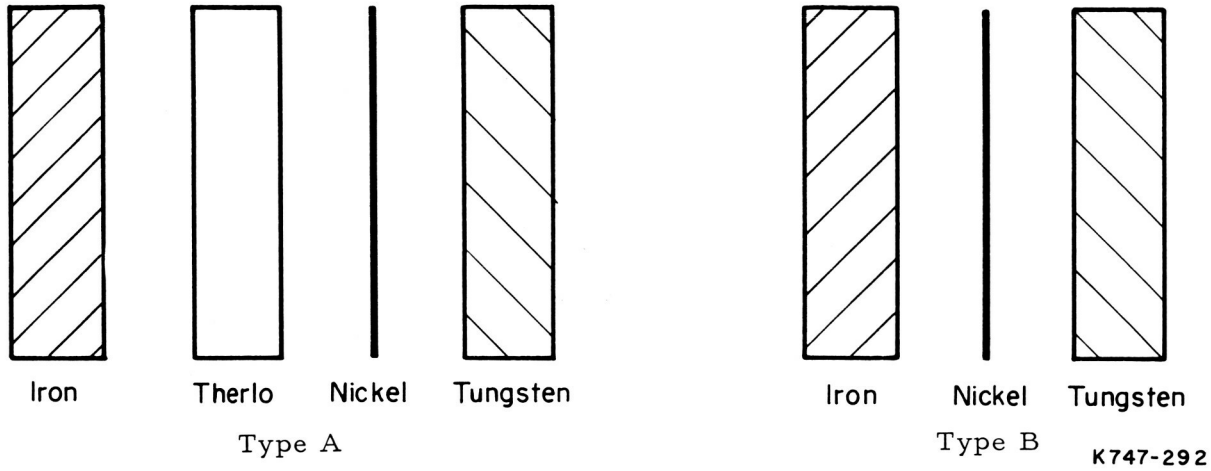

FIGURE 8. BASIC APPROACHES TO TRANSITION-MEMBER JOINING

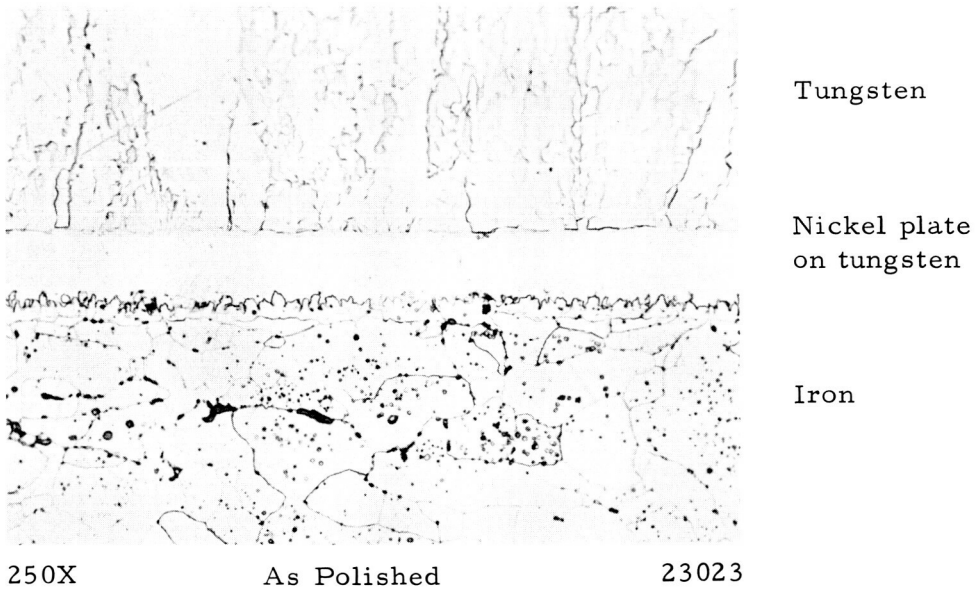

FIGURE 9. IRON-NICKEL-TUNGSTEN BOND FORMED BY HOT ISOSTATIC PRESSING AT 1400 F, 10,000 PSI

more suitable for fabrication. Figure 9 shows a photomicrograph of a resulting bond in the Type B material combination produced at 1400 F and 10,000 psi. Temperatures of 1200 and 1400 F and pressures of 2500 and 10,000 psi were used in bonding trials with both material combinations, but only the higher temperature and pressure combination was found to produce adequate bonds.

Bonding of iron to tungsten with nickel, when attempted at 1200 F, was entirely unsuccessful. The quality of bonds produced with a lower pressure of 2500 psi at 1400 F was mechanically poor. The bonding was spotty, leading to separation under a light force. Bonds of this type failed completely during three cycles when subjected to thermal cycling from room temperature to 950 F. Resistance of the bonds produced at 1400 F and 10,000 psi to similar thermal cycling remains to be demonstrated. The nickel in the specimen shown in Figure 9 was incorporated as a plated coating on the tungsten. Similar bonds were obtained with the nickel applied in the form of 1-mil-thick foil. The latter is preferred because of the variability found in the quality of nickel plates on tungsten. Laminated nickel plate was found to remain completely unbonded during the pressure-bonding cycle.

The prime difficulty with the material combination of Type A occurred at the Therlo-nickel-tungsten bond. Bonding of the constituents was achieved, but the Therlo-to-nickel bonds separated as shown in Figure 10. A nickel diffusion zone, although not clearly apparent in the photomicrograph, existed in the surface of the Therlo, giving evidence of initial bonding. The area photographed was selected to show where the nickel remained bonded to the Therlo and was torn free from the parent material. The failure was attributed to a weak bond between the nickel and Therlo and the relatively high strength of the differentially contracting tungsten and Therlo members. The success with the iron-to-tungsten bonds in Type A is attributed to the quite low strength of the pure-iron-powder product.

Satisfactory bonds were obtained between iron and the Therlo member without the use of a bonding agent as is shown in Figure 11.

The iron-nickel-tungsten Type B combination appears to provide a suitable transition member, when fabricated at 1400 F and 10,000 psi, if such a fabrication schedule is found to be compatible with the other aspects of the segmented element.

Tungsten-SiGe Bonding

Since the state-of-the-art bond between tungsten and SiGe has a temperature limitation of about 1000 F, several approaches were explored to produce this junction. They involve joining during total element fabrication or by an alternative route where this junction is made prior to incorporating the SiGe segment in the element. The approaches evaluated follow three primary paths as outlined below.

(1) Production of the tungsten-SiGe bond at a relatively high temperature (1400 F) by direct reaction or braze bonding under the pressure conditions of the hot-isostatic-pressing process. The segmented element would be produced completely in this one-step operation. The time of bonding might be sufficiently short to prevent damage to the SiGe by reaction with the tungsten.

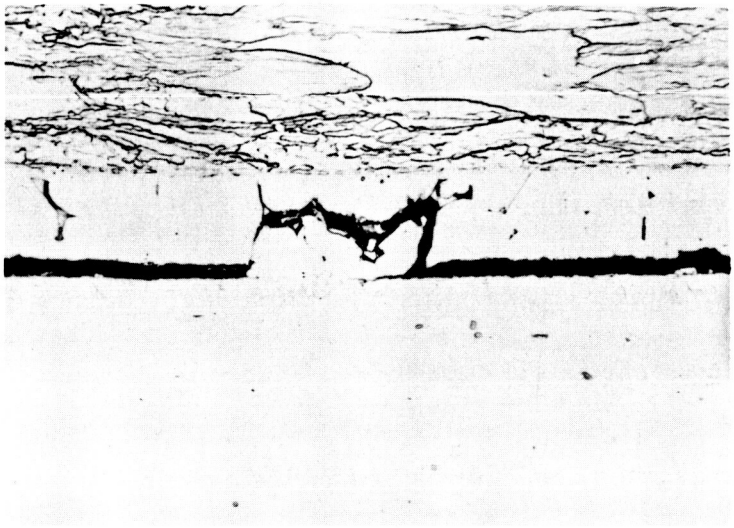

FIGURE 10. TUNGSTEN-NICKEL-THERLO ALLOY BONDS FORMED BY HOT ISOSTATIC PRESSING AT 1400 F, 10,000 PSI

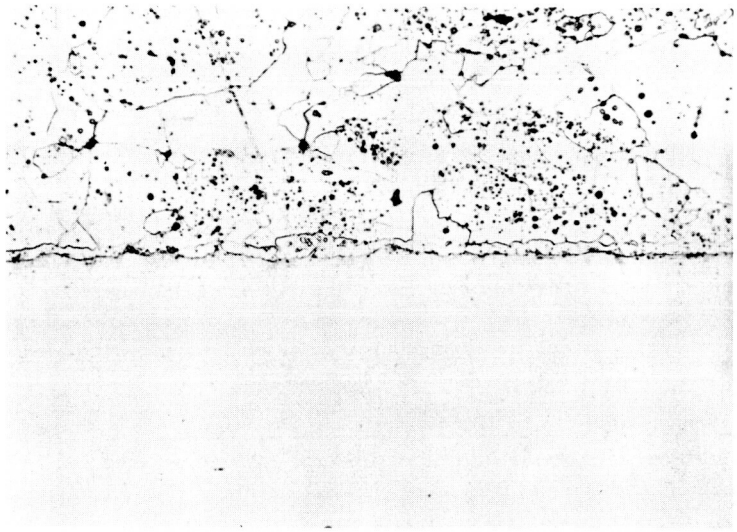

FIGURE 11. IRON-THERLO BOND FORMED BY HOT ISOSTATIC PRESSING AT 1400 F, 10,000 PSI

(2) Join the SiGe segment to the tungsten member of the prefabricated PbTe segment by means of a low-temperature (less than 1000 F) eutectic braze which might be accomplished with gold. Gold forms eutectics with both silicon and germanium at temperatures near 700 F which is below the normal operating temperature (about 975 F) of this junction.

(3) Produce a braze bonded tungsten-SiGe composite which will survive subsequent pressure bonding at temperatures of about 1000 F.

The information relating to these three areas of investigation is discussed below.

Tungsten to SiGe Joining During Pressure Bonding

Attempts to produce a direct reaction bond at the conditions which are considered the maximum applicable for segmenting, namely 1400 F and 10,000 psi, were completely unsuccessful. In no instance was there any signs of attack or sticking together of the members. Although the hot-isostatic-pressing container is evacuated prior to use, the atmosphere within is apparently insufficiently clean to maintain the necessary cleanliness of bonding surfaces. The mica used for element encasements is a flake-type product which is a prime source for occluded gases.

Similar attempts made under the same conditions with gold as an eutectic-forming braze were also unsuccessful. This approach was pursued no further.

Low-Temperature Gold Braze. The use of gold as a braze agent for joining the tungsten to SiGe was first considered as a possible means of accomplishing the joining at a temperature below 1000 F. The gold-silicon or gold-germanium eutectic reactions which occur at about 700 F might possibly be utilized in producing bonds, in place, during normal operation of the couple or in a separate brazing operation. Either approach could then be used to join the SiGe segment to a prefabricated PbTe segment which has the transition member attached.

Attempts to effect such a bond at 1000 F in either argon or hydrogen atmospheres were unsuccessful. Reaction between the gold (in the form of foil) and SiGe occurred only spottily at apparent localized points of pressure contacting, causing small holes to be formed in the gold foil. The inability to react the member was attributed to the presence of a thin film of silicon dioxide (SiO_2) on the surface of the SiGe.

Several attempts were then made to effect the braze with the aid of potential fluxing agents. Although the temperature was low for titanium hydride it was used in a thin slurry over the SiGe surface for the purpose of providing at least a small source of nascent hydrogen for oxide reduction. No improvement was achieved. The use of ammonium bifluoride at the bond surface as a source of HF and F_2, which are effective reactants with SiO_2, produced partial successes on a random basis. The best result involved effective brazing of about one-third of the surface of an 0.3-inch-diameter specimen.

This approach was pursued no further.

High-Temperature Braze. With the lack of success in evolving a low-temperature brazing schedule with gold as the braze material, the temperatures required to effect a braze in argon and vacuum were determined. Sound brazes were produced in both argon at 2000 F and in vacuum at as low as 1475 F. Vacuum was selected for use in preparing test specimens to take advantage of lower temperatures, but a braze temperature of 1800 F was found to be more reliable in making reproducible brazes. Figure 12 shows a photomicrograph of the gold-brazed tungsten-SiGe composite.

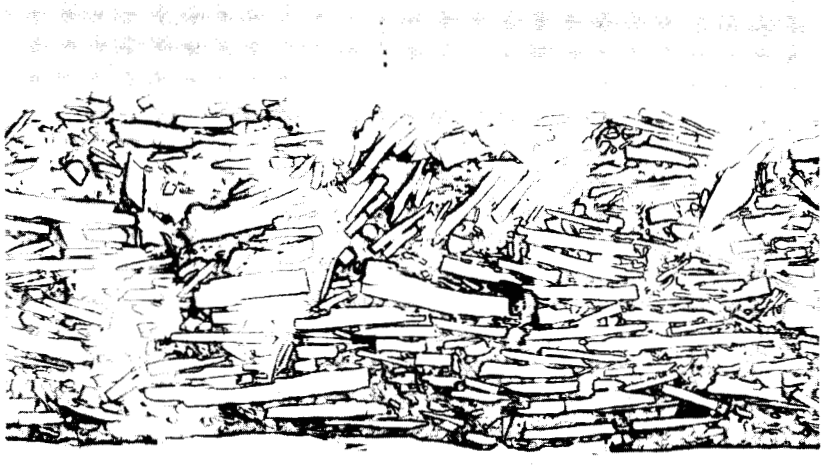

250X 23363

FIGURE 12. GOLD-BRAZE BOND OF TUNGSTEN TO SiGe MADE IN VACUUM AT 1475 F

The gold-brazed composite was evaluated for its compatibility with a high-temperature element fabrication schedule by processing specimens through a typical 1400 F pressure-bonding cycle of 1 hour's duration. This treatment caused complete separation of the tungsten shoes. The separation occurred at the bond interface with no tear-out of SiGe, indicating a weak bond to the tungsten. The gold was then replaced by a gold-nickel alloy braze to improve the potential for bonding to the tungsten with the addition of nickel. The as-brazed bonds were equal in quality to those obtained with gold, but were more serviceable. The suitability of this type of bond was evaluated by means of a 1-hour furnace treatment at 1400 F. Satisfactory results were obtained in this case. Figure 13 shows a photomicrograph of the braze area after the additional thermal treatment. The bond area consists of a uniform, homogenized band of reaction product. No cracks were apparent in the SiGe.

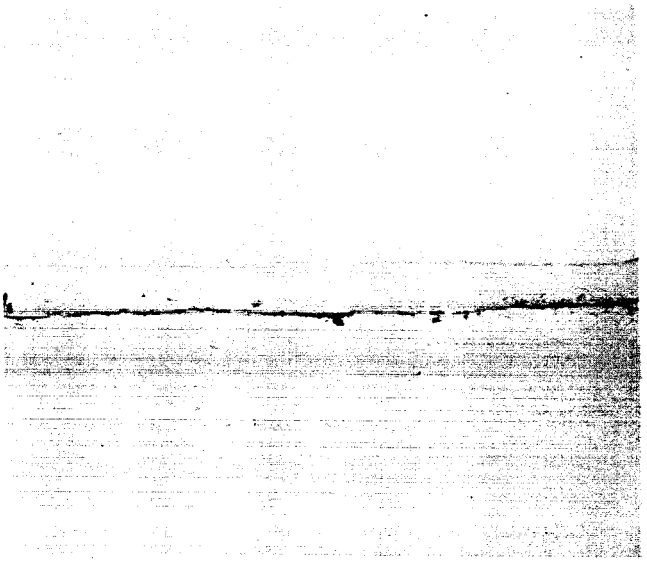

FIGURE 13. GOLD-NICKEL ALLOY BRAZE OF TUNGSTEN TO SiGe PERFORMED AT 1800 F IN VACUUM.

Specimen was thermally aged 1 hour at 1400 F.

Lead Telluride Segment Fabrication and Evaluation

The lead telluride segment in this study consists of the thermoelectric material with shoes attached at either end. The hot-isostatic-pressing process was selected for fabrication of this segment, its selection being based on the following considerations.

(1) The process as applied by Battelle has been shown to be capable of producing PbTe thermoelements of good quality from powder starting materials.

(2) The process is effective in producing strong and well-bonded element-shoe composites from all powder starting materials.

(3) The range of processing temperatures over which PbTe elements can be fabricated is greater than for any other process. Applicability over the range 750 F to 1400 F has been demonstrated.

(4) The above-listed features can be combined with an effective pressure-bonding capability useful for joining other members of a segmented element.

(5) The process is not as restricted by 1/d ratio limitations as are some fabrication processes such as hot die pressing.

Segment Preparation

The materials of the PbTe segment were incorporated entirely in powder form. The PbTe was -100 mesh and iron as the reference shoe material was -200 + 270 mesh. A second shoe material was studied and is discussed later in the report.

The segment composite was prepared for hot isostatic pressing by first preparing a green-pressed body. The shoes were firmly attached to the PbTe in the green form by layering the powders in the die and pressing them together. A low pressure, approximately 10,000 psi, was used to form each layer in the die before the next layer was put atop the previous one. The final pressing was performed at 100,000 psi. Sufficient interlocking of the iron and PbTe powders occurs to make a strong mechanical bond. The green-pressed segment was slipped into a preformed mica sleeve and then encased in an evacuated thin-wall stainless steel container for hot isostatic pressing.

A round-shaped element was initially selected for development, but later a square shape was used to achieve better deformation characteristics. During pressing, the element container collapses onto the specimen and, as a result of the initial clearances and reduction in thickness of the element and mica sleeve, the can attempts to reduce in perimeter. In the case of the round can, wrinkles form in the surface which are roughly duplicated in the element surface. This was considered objectionable because of the variation in cross section which occurs randomly along the element. In addition, the can tends to bend and this can conceivable cause breaking of the specimen. In the case of the square container, the deformation is quite uniform with the excess can material moving to the corners causing them to sharpen. The sides of the square element develop a gentle concave shape which has not been found objectionable.

Segment-Material Characteristics

The structural condition of the hot-pressed PbTe segments was examined to determine the effects of the pressing temperature. The two temperatures of prime interest were 900 F and 1400 F. The metallographic specimens were studied in the as-polished condition under bright-field illumination with particular attention given to density, shoe-element reaction products, and cracking.

Both the p- and n-types of PbTe are effectively consolidated to a high density at 900 F and 2500-psi pressure. Representative photomicrographs are shown in Figures 14 and 15. After pressing at 1400 F and 2500 psi, the p-type PbTe contains a considerable amount of porosity as exemplified in Figure 16. The porosity in the p-type PbTe pressed at 1200 F is similar but is not as great. Although the porosity in p-type PbTe pressed at 1400 F is quite extensive, it has no apparent effect on the electrical properties, this conclusion being based on the property characterizations presented in an earlier section.

The porosity is attributed to entrapped gas from the green-pressing operation and possibly volatile surface oxides. When pressed at 900 F, the PbTe is sufficiently strong to resist creep growth of the pores during the short period over which the pressure is released at the pressing temperature, thus producing a dense structure. In the case of the 1400 F pressing condition, the PbTe is so weak when the pressure is released at temperature that the high-pressure gas in the pores can cause the surrounding material to creep.

100X As Polished 26103

FIGURE 14. p-TYPE PbTe FABRICATED AT 900 F

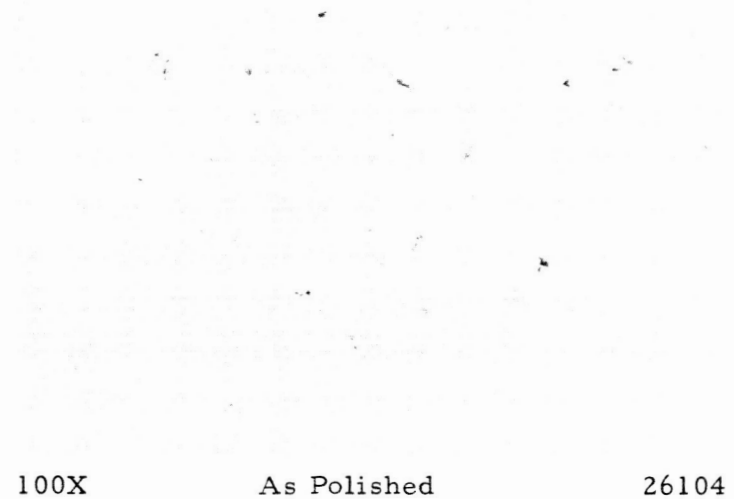

100X As Polished 26104

FIGURE 15. n-TYPE PbTe FABRICATED AT 900 F

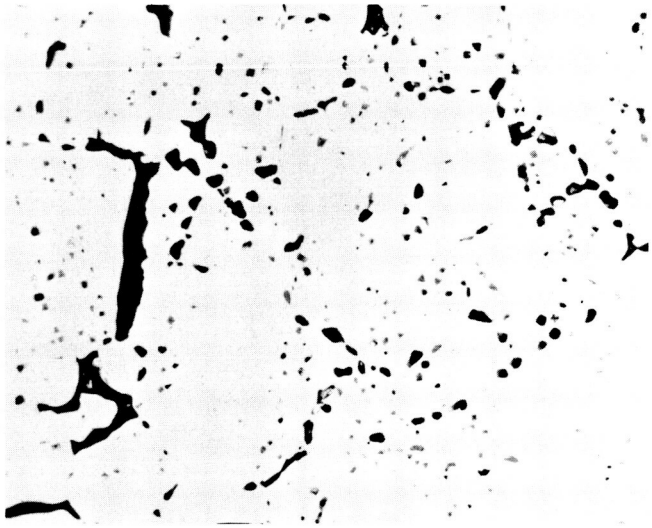

250X As Polished 23364

FIGURE 16. STRUCTURE OF p-TYPE PbTe HOT ISOSTATICALLY PRESSED AT 1400 F

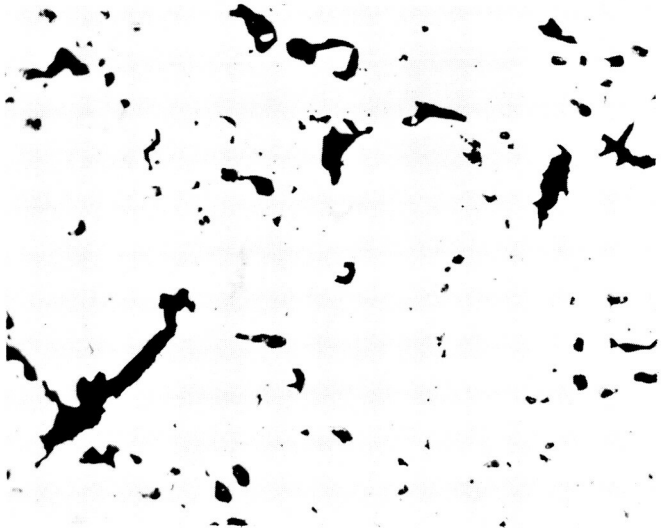

250X As Polished 25300

FIGURE 17. STRUCTURE OF p-TYPE PbTe AFTER AGING AT 950 F

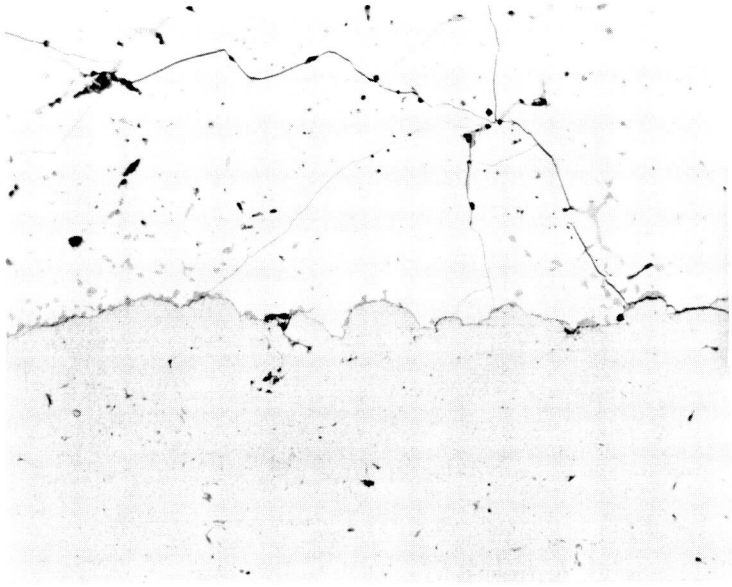

250X As Polished 23366

FIGURE 18. IRON - 2p PbTe BOND PRODUCED AT 1400 F SHOWING Fe - PbTe REACTION PRODUCTS AND CRACKING OF PbTe

Evidence of this was found in p-type PbTe pressed at 900 F or lower which is subsequently aged for a prolonged time at a temperature of 950 to 1000 F. Significant porosity is generated, as exemplified by the specimen shown in Figure 17. In this case the porosity also had no apparent effect on element performance. The n-type PbTe exhibits similar behavior, but to a much smaller degree. The total void volume is smaller and the pores tend to coalesce at the grain boundaries.

The bonds between Tegs 2 PbTe and iron fabricated at both 1400 F and 900 F were examined metallographically. Reaction of the iron with the p-type PbTe was observed in specimens pressed at both temperatures. Figure 18 shows the reaction product present near the bond interface in a 1400 F specimen. The new phase is believed to be iron telluride. Microprobe analysis performed on a path across the interface shows localized concentrations of iron and tellurium in the PbTe near the interface, with accompanying depletion of lead. The specimens pressed at 900 F show smaller amounts of the new phase, while n-type PbTe shows no evidence of such reaction at either temperature.

Because of the notably great propensity of p-type PbTe (Tegs 2) to crack under stress, the relative effects of pressing temperature and pressure on cracking were examined. Earlier experience by Battelle with hot isostatic pressing has shown that p-type PbTe can be overpressed at 900 F. A pressure of 10,000 psi causes internal stresses in the material making it extremely sensitive to cracking. Pressing was attempted at 10,000 psi and 1400 F, however, so that the higher temperature might allow the stresses to relax before the specimen was cooled. This was found not to be the case, and extensive cracking still occurred. With a pressing schedule involving 1 hour at 10,000 psi followed by 2 hours at 2000 psi to permit relief of the overpressing, the material showed improvement but cracks of the type shown in Figure 18 were prominent and the bulk material was abnormally sensitive to stress. In addition, the shoes were easily broken free from the elements. It is not known whether the cracks in the latter case actually resulted from overstressing or from the large temperature change and resulting differential expansion in cooling to room temperature.

A pressure of 2500 psi was established for pressing of p-type PbTe at all temperatures. N-type PbTe has shown no readily apparent sensitivity to pressing at pressures to 10,000 psi.

Element-Shoe Testing

The selection of iron as the shoe material for PbTe is based primarily on its accepted chemical compatibility and ability to be bonded to PbTe. To date, the major problem associated with iron results from its insufficiently high expansion rate. It is about 30 percent lower in expansion rate than PbTe, causing the PbTe to undergo tensile stressing upon cooling from the bonding or operating temperature. In the case of the very fragile p-type (Tegs 2) PbTe, cracking becomes a serious problem. The two considerations given to this problem with the p-type material were: (1) determination of the relative effects of pressing temperature on the presence of cracks, and (2) evaluation of a higher-expansion-rate, iron-base alloy as a possible replacement for iron.

The bonded specimens prepared for this study were evaluated by means of resistance traverse measurements made across the bond interfaces and the adjacent thermoelectric material. These measurements were made with the apparatus shown

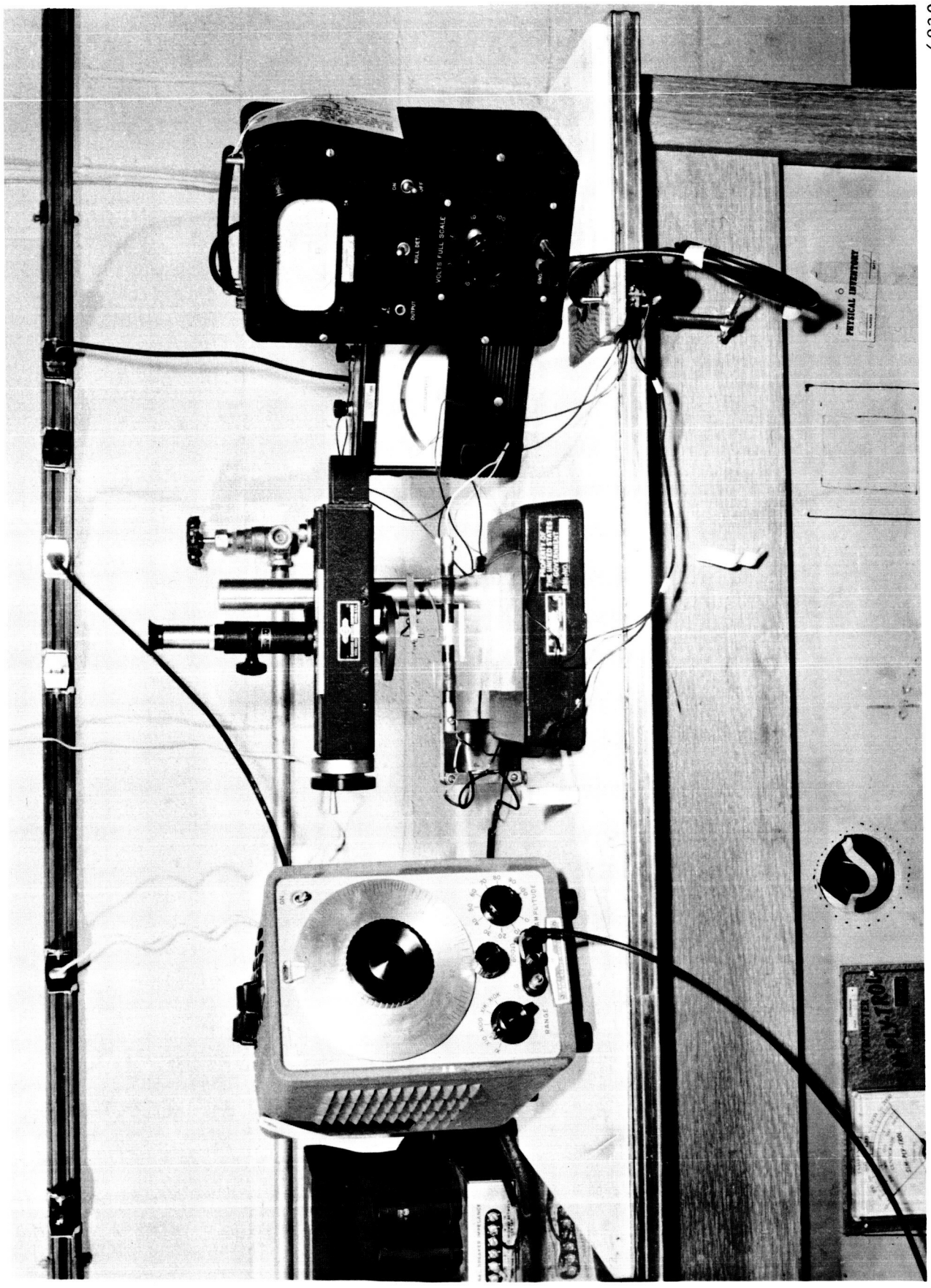

FIGURE 19. RESISTANCE-TRAVERSE APPARATUS

in Figure 19. The specimen is held between contact electrodes while an a-c current of about 0.7 ampere is passed through. A calibrated screw drive mechanism is used to locate accurately a voltage probe at precise points along the specimen. The voltage drop between the probe and a fixed end electrode is measured at each probe location by means of a vacuum-tube voltmeter. The current is determined by measuring the voltage drop across a calibrated resistor. The calculated resistance values are plotted as a function of probe traversing distance. The increments of distance between probe locations in the vicinity of the bonds was 10 mils. Figure 20 shows examples of a "good" and a "poor" specimen of p-type PbTe (Tegs 2) with iron shoes attached that had been hot pressed at 1400 F. The sharp discontinuity in the poor specimen indicates a sharp rise in resistance as the result of a crack.

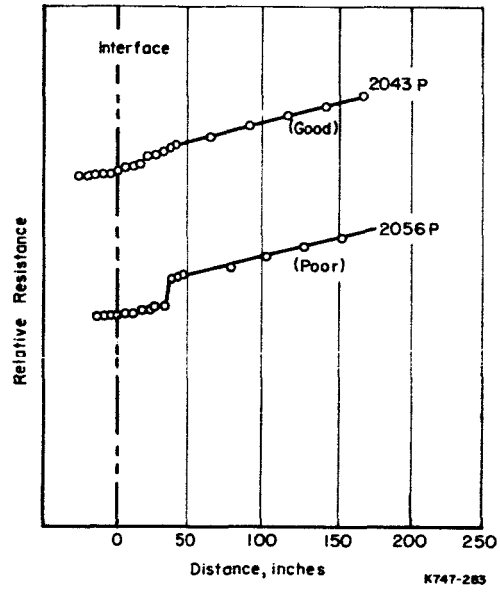

FIGURE 20. EXAMPLES OF BONDED PbTe SPECIMENS BASED ON RESISTANCE-TRAVERSE MEASUREMENTS

Effect of Pressing Temperature. Examination of resistance traverses of p-type specimens pressed at 1400 F and 900 F show the higher temperature to yield generally larger and more frequent discontinuities. This was supported by the observed greater frequency in the higher temperature specimens of shoes being separated from the elements upon decanning. On the basis of these results, the 900 F pressing temperature is to be preferred for the p-type material.

The Tegs 3p PbTe was also fabricated into specimens for resistance traversing but the extremely high degree of shoe separations obviated their inclusion in the test program. Two attempts to incorporate the Tegs 3p material were unsuccessful for lack of bonding. Tegs 3p-type PbTe was consequently eliminated from consideration in segment fabrication. Its relatively low power factor supported this decision.

Because of the less-problem-producing characteristics of the Tegs 2n-type PbTe, it was excluded from this traverse study. Random traverses and metallographic examinations performed on specimens pressed at 900 and 1400 F, however, have shown no apparent difference in bond characteristics or element cracking tendencies. Cracks have seldom been detected in as-pressed n-type specimens. Temperatures in the range 900 to 1400 F are considered equally acceptable for the n-type PbTe fabrication.

Iron-Base-Alloy Evaluation. An alloy of iron-8 percent tin (designated BMI-8) investigated by Battelle was found to have an expansivity greater than iron, placing it between iron and PbTe. Since tin is commonly alloyed with both p- and n-type PbTe in the form of tin telluride, its presence in an iron shoe was considered to be potentially acceptable. On the basis of these factors, the alloy was evaluated against iron as a shoe material that might reduce cracking and possibly increase the life characteristics of the junction with PbTe.

The BMI-8 alloy was prepared by arc casting and was converted to powder by filing. Two powder sizes were prepared by milling in a mortar and pestle: -100 +270 mesh and -270 mesh. The test specimens were die pressed and hot isostatically pressed at 1400 F in a like manner with specimens containing iron shoes of -200 +270-mesh powder.

The fabricated specimens were traversed and then subjected to thermal aging in argon at 950 F. The aging was performed in three periods to provide these thermal cycles to room temperature. Resistance traverses were performed after each cycle. A total of 263 hours were accumulated at the aging temperature. The following observations were made as a result of this study.

(1) The fine, minus 270-mesh, alloy powder consolidated well, while the coarse, -100 +270-mesh, powder did not. The coarse shoes tended to crumble at their edges.

(2) The shoes made of coarse powder (poorly densified) showed the greatest tendency to remain intact on the specimens during cycling.

(3) The frequency of cracks or discontinuities in the traverse curves and the response to cycling among the three groups of specimens were essentially alike. The results showed no preference for either shoe material.

(4) The general effect of cycling was to create and/or increase the magnitude of each discontinuity in the traverse curve. Figure 21 shows an example of the effect of cycling and aging on the resistance-traverse curves of a BMI-8 specimen.

On the basis of these results, the following conclusions were drawn:

(1) Iron should be used for element fabrication until such time that the BMI-8 alloy, which is under investigation in other studies, is shown to offer merit.

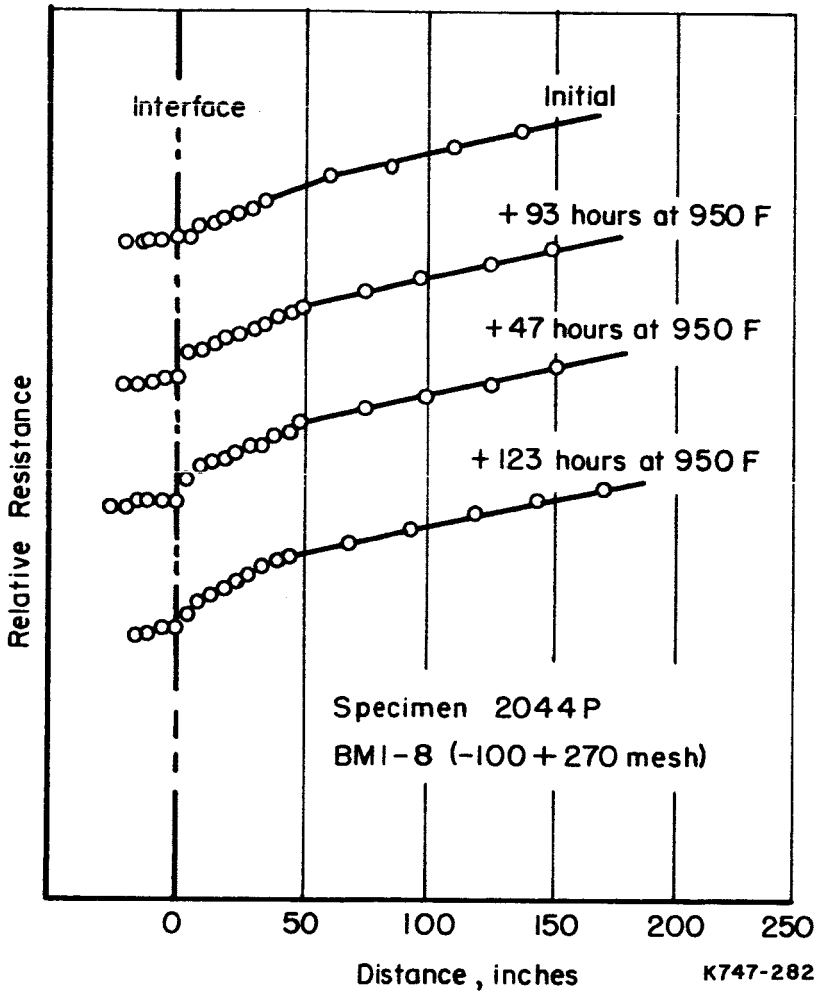

FIGURE 21. EFFECTS OF THERMAL CYCLING AND AGING ON RESISTANCE TRAVERSES FOR p-TYPE PbTe

(2) The high temperature of hot pressing (1400 F) and/or the thermal-cycle test may have imparted conditions too severe to show differences in shoe performance.

Concurrent with the above investigation, tests were initiated to ascertain whether the BMI-8 alloy is in fact free of adverse poisoning effects. The compatibility tests were performed on PbTe test specimens with iron and BMI-8 as separate powder additives to the p- and n-type PbTe. One weight percent additions were used and the specimens were hot isostatically pressed at 900 F. Elevated-temperature Seebeck-coefficient and room-temperature-resistivity determinations were made after pressing and after thermally aging for 70 hours at 950 F. The results are compared in Table 2.

The n-type PbTe shows no significant difference in the properties while the p-type PbTe shows a strong effect of aging that is approximately the same for both additives. The difference in values produced by the two additives is believed to be insignificant because of the magnitude of the change from the original values. Additional aging is being performed to provide more meaningful information. The increase in resistivity observed in the p-type PbTe may be the result of the reaction of iron to form iron telluride.

Segmented Element Fabrication

The information generated in the aforementioned supporting studies, where the different parts of the segmented element were considered separately, was used to establish potential schemes of element fabrication and element configurations. The term configuration as used here applies to identification of the kinds and array of makeup materials in a particular element. Once a configuration has been established, trial fabrications are attempted to assess the validity or practicality of the various factors involved. During this report period, four fabrication schemes and four associated configurations were devised. They are shown schematically in Appendix D.

Fabrication Scheme A involves pressure bonding of the PbTe segment and transition and subsequent gold brazing of the tungsten shoe to the SiGe segment. This was shown earlier in the report to be an invalid approach because of the inability to overcome the inhibiting action of the oxide film on the SiGe at a temperature below 1000 F.

Fabrication Scheme B incorporates a gold-nickel prebraze of the tungsten to the SiGe segment. It was demonstrated that this type of braze could withstand a 1-hour aging at 1400 F without damage to the SiGe. The feasibility of joining the PbTe segment and iron shoe to the tungsten using nickel in a 1-hour, 1400 F hot-pressing step was also demonstrated. The sequential application of brazing and then hot pressing should accomplish the joining of these segments. Since a 10,000-psi pressure is required to produce the nickel bonds, this scheme was considered useful only on the n-type element. The problems of cracking of p-type PbTe at 1400 F and the fragility resulting from pressing at 10,000 psi provide the basis for its exclusion from Scheme B.

An attempt was made to produce the n-type element by Scheme B. Figure 22 shows a photograph of the resulting product. The surfaces were ground to make the transition member more readily observable. A crack clearly shows in the SiGe above the bond interface. It was not apparent whether the crack resulted from tungsten-SiGe

TABLE 2. EFFECTS OF SHOE-MATERIAL ADDITIVES ON THE ELECTRICAL PROPERTIES OF PbTe

Additive, weight percent	Initial Properties After 900 F Pressing		Properties After Aging 70 Hours at 950 F	
	Resistivity[a] μohm-cm	Seebeck Coefficient[b], μv/C	Resistivity[a], μohm-cm	Seebeck Coefficient[b], μv/C
P-type PbTe				
1 Fe	538	224	1210	276
1 BMI-8	627	237	1480	267
N-type PbTe				
1 Fe	677	240	647	232
1 BMI-8	627	226	647	228

(a) Room temperature.

(b) Average between 150 and 500 C.

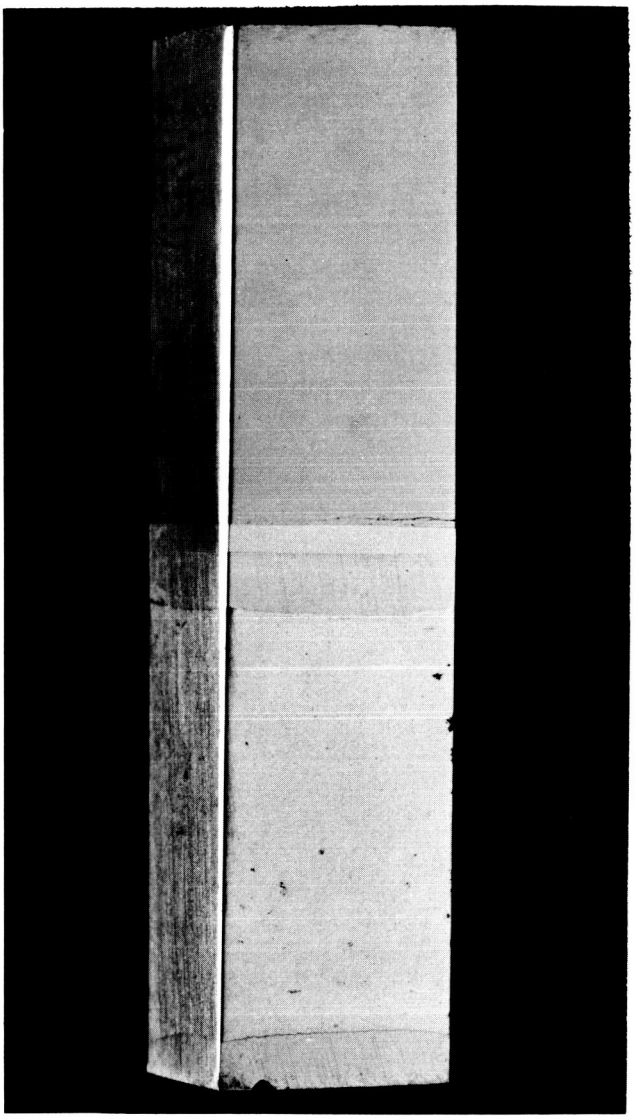

FIGURE 22. n-TYPE SEGMENTED SiGe-PbTe ELEMENT FABRICATED BY SCHEME B

reaction or bending stresses during the cool-down period after pressing. The specimen will be examined metallographically to aid in determining the cause of the crack. Additional specimens of this type will be prepared to provide additional information on the suitability of Scheme B.

Fabrication Schemes C and D are based on the use of a 900 F, 2500-psi hot-isostatic-pressing schedule which is applicable to both the p- and n-type PbTe. The SiGe will be joined to the tungsten by either direct reaction or brazing with gold-nickel alloy. Either type of bond should survive the following 900 F treatment. In both cases the tungsten will be simultaneously joined to a nickel shoe with gold as the braze agent. This braze has not been demonstrated in this work but is considered essentially standard technology. The final joining of the prebrazed SiGe segment to the PbTe segment will be accomplished using tin as a braze. This type of junction is produced as standard practice by Battelle in its thermoelectric work. The validity of these choices will be determined in planned fabrication trials of these schemes.

To this point, nothing has been said about joining the p- and n-type elements into a working couple. The plan is to join the elements with a silicon-alloy hot strap during installation and heat-up of the elements during couple test. Gold will be used as the brazing agent. The braze will be accomplished at the planned hot-junction temperature of about 1700 F (~ 1200 K). Figure 23 shows a photomicrograph of such a junction made at this temperature in an argon atmosphere simulating the couple test environment.

250X 24564

FIGURE 23. SiGe BRAZED WITH GOLD AT 1700 F IN ARGON

Summary

Several fabrication schemes which show potential feasibility for segmenting of SiGe and PbTe were derived on the basis of integrating information from separate fabrication studies of the components of the element. The resulting schemes are

based on fabrication approaches which circumvent apparent materials and processing incompatibilities.

A transition member of tungsten joined to iron with nickel as bonding agent requires a temperature of 1400 F and a pressure of 10,000 psi. These conditions are compatible with n-type PbTe fabrication but not with the p-type; therefore, a scheme based on these parameters is applicable to fabrication of the n-type element only. The p-type element must be fabricated by a scheme involving hot pressing at about 900 F.

On the basis of the successful 1400 F aging for 1 hour of a gold-nickel alloy brazed tungsten-SiGe composite, the fabrication scheme mentioned above for the n-element appears feasible. The gold-nickel alloy braze also provides a means for fabrication at 900 F and is applicable to both p- and n-type elements.

The electrical-property characterization of the 900 F and 1200 F isostatically consolidated PbTe shows either temperature to be applicable for segmenting purposes.

Comparison testing between Fe and BMI-8 shoe materials showed the latter to exhibit no decided advantage over iron. These data are subject to further verification.

TASK III. DEVELOPMENT OF A THERMAL INSULATION AND SUPPORT STRUCTURE

Objective

The objective of this task is to fabricate and test a selected grouping of heat-source support and thermal-insulation structures in order to obtain their thermal and mechanical properties. On the basis of these data, a correlation with analytical predictions will be made to define and extend the relations describing performance of the insulation.

Scope of Work

The scope of this development work includes the fabrication, thermal testing, structural testing, and performance correlation of a selected group of insulation structures. Gas-pressure bonding of the insulation structures was accomplished during the period covered by this report. As a prerequisite to gas-pressure bonding, experiments for optimization of the bonding process were completed, fabrication of the insulation components was planned, and the components were assembled into structures.

Design of Insulation Structures

Hastelloy C was chosen as the candidate material for fabrication of the insulation structure. This material was chosen for its high-temperature strength and low thermal conductivity. The finished sample structures, 3 inches in diameter, consisting of five foil-and-web layers, were generated from 3-1/2-inch-square sections made by diffusion bonding. In this process, the complete unbonded structure was compressed under vacuum, at high temperature, for an adequate time to effect complete diffusion bonding.

The insulation structure is pictured in Figure 24. The parameters are shown in Figure 25 where:

L = web-bend length
H = web height
t = web thickness
f = foil thickness.

Two series of structures are being fabricated, covering two ratios of web-bend length to web height. Within each series, structures are selected that combine three foil thicknesses and three web thicknesses. For Series 1, the web-bend length is 1 centimeter and that for Series 2 is 1/2 centimeter. For all specimens, the foil spacing, or web height, is 0.05 inch. These size combinations represent expected extremes of strength, weight, and thermal resistance. Nine structures are being produced in each series, as shown in Table 3. Each structure will have a 1/16-inch-thick end plate on both sides to facilitate testing procedures.

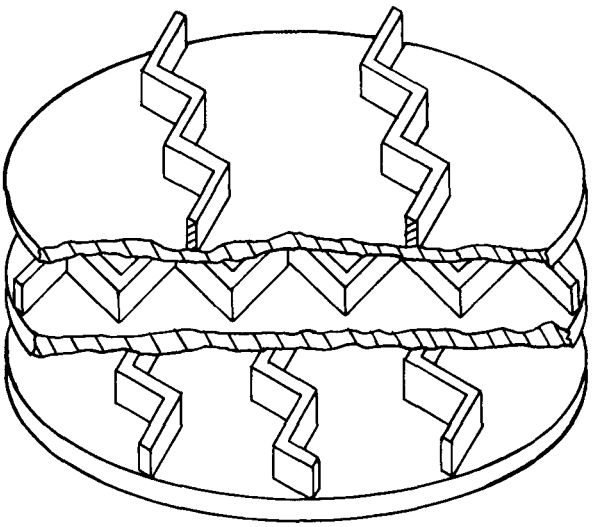

K747-277

FIGURE 24. METALLIC-INSULATION STRUCTURE

TABLE 3. COMPONENT DIMENSIONS FOR INSULATION STRUCTURES

Structure	Web Thickness, mil	Foil Thickness, mil
1	0.004	0.004
2		0.008
3		0.012
4	0.008	0.004
5		0.008
6		0.012
7	0.012	0.004
8		0.008
9		0.012

The work thus far accomplished in fabricating the insulation structures may be discussed in terms of three efforts: the bonding process optimization, the fabrication of the structural components, and the subsequent assembly and bonding of these components into structures.

Bonding-Process Optimization

Past experience at Battelle has demonstrated the feasibility of using the gas-pressure-bonding process to fabricate honeycomb and honeycomb-like structures from

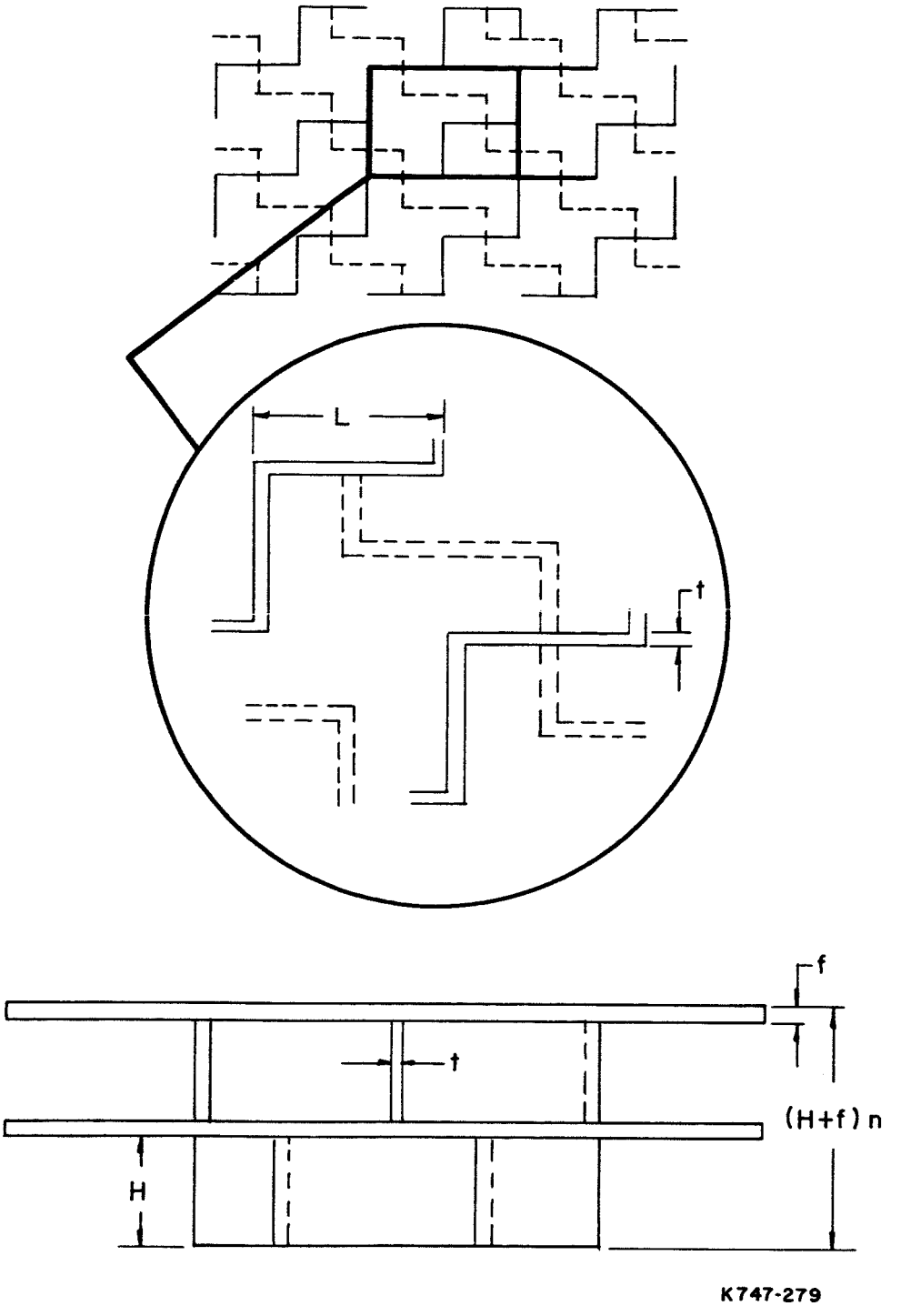

FIGURE 25. REPEATING SECTION OF INSULATION STRUCTURE SHOWING DIMENSIONAL PARAMETERS

a wide variety of engineering materials. Predicting the optimum self-bonding parameters for most engineering materials in many cases would not be a difficult task. But, since the fabrication concept involves the use of an expendable tooling to maintain structural integrity at the high pressure and elevated temperature of bonding, the selection of bonding-process parameters becomes dependent not only on the quality of the bond achieved but also on the effects of interaction of the leachable tooling with Hastelloy C, the alloy chosen by design for the structural insulation. The bonding parameters were chosen to maximize the quality of the Hastelloy C self-bond and minimize the diffusion reaction between the leachable tooling and Hastelloy C. A minimum of diffusion interaction between Hastelloy C and the candidate tooling is necessary because the tooling is eventually acid leached from the Hastelloy C. A large reaction zone between Hastelloy C and the tooling would result in a rough Hastelloy C surface after leaching, increasing the emissivity of the parallel foils in the final structure. Because the magnitude of these problems was unknown, an experimental program was initiated to generate data that could be used to aid in the selection of the bonding-process parameters and the materials system. The experimental objectives were the following and will be discussed in that order:

(1) Establish bonding parameters for Hastelloy C

(2) Evaluate and select candidate leachable tooling materials

(3) Determine which of several selected acid solutions will effect the most efficient tooling removal

(4) Examine techniques which might be applicable to the polishing of a final bonded and leached structure.

From past experience and a study of the available literature, experimental specimen configurations were designed to help screen and select the best possible materials system and bonding parameters with the least number of experimental process cycles. The specimen configurations and process conditions, along with the purpose of the specimen, are shown in Figure 26.

Initially, duplicate specimens were made of Configurations 1, 2, and 3 for bonding at 2100 F and 10,000 psi for 3 hours. These initial bonding conditions were chosen because they had proved successful in bonding other iron- and nickel-base alloy systems. Nickel and iron were chosen as the tooling because they are relatively inexpensive, are stable at the expected bonding-temperature range, and are readily dissolvable in a variety of common acids that do not attack Hastelloy C.

The chrome plating in Configuration 2 and platinum foil in Configuration 3 were selected to serve as a diffusion barrier in the event that neither plain iron nor nickel in Configuration 1 proved to be suitable.

The Hastelloy C in Configurations 2 and 3 was prepared for bonding by dipping in a solution of 50 parts nitric acid, 10 parts hydrofluoric acid, and 40 parts water until the surface was etched to a light satin finish.

The nickel-plated Hastelloy C in Configuration 1 was prepared by dipping in a hot alkaline cleaning solution. After acid or alkaline cleaning, each piece was rinsed in distilled water and ethyl alcohol. The iron- and nickel-tooling pieces, as well as the tooling with chrome plate and platinum foil, were prepared by scrubbing in a hot alkaline solution, followed by rinses in distilled water and ethyl alcohol. During assembly all components were handled with white gloves and tongs and/or tweezers.

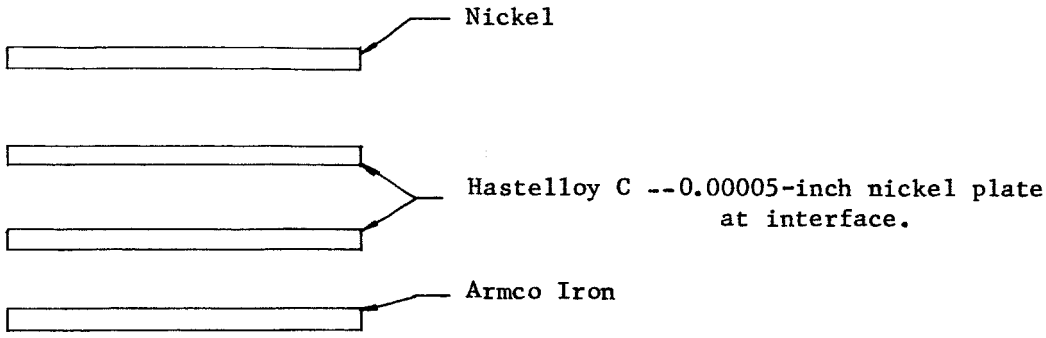

(a) Bonding Coupon Configuration 1
Purpose: Evaluation of Hastelloy C self-bond employing nickel plate as a diffusion aid.
Evaluation of reaction between Hastelloy C and candidate iron and nickel tooling.

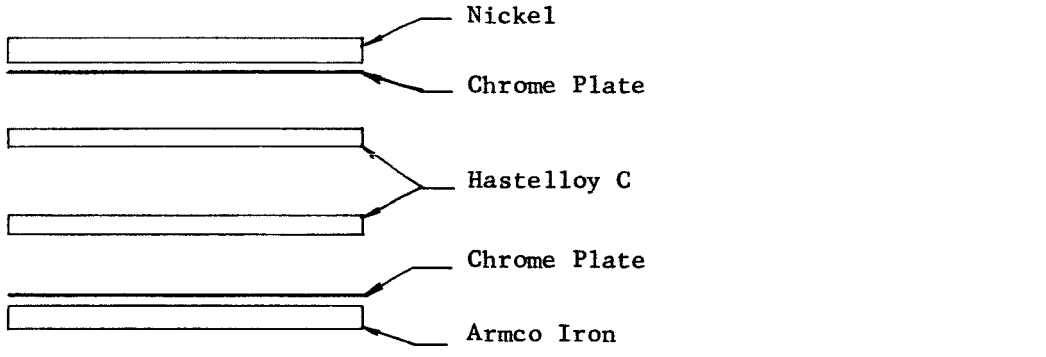

(b) Bonding Coupon Configuration 2
Purpose: Evaluation of Hastelloy C self-bond.
Evaluation of reaction between Hastelloy C and chrome-plated iron and nickel tooling.

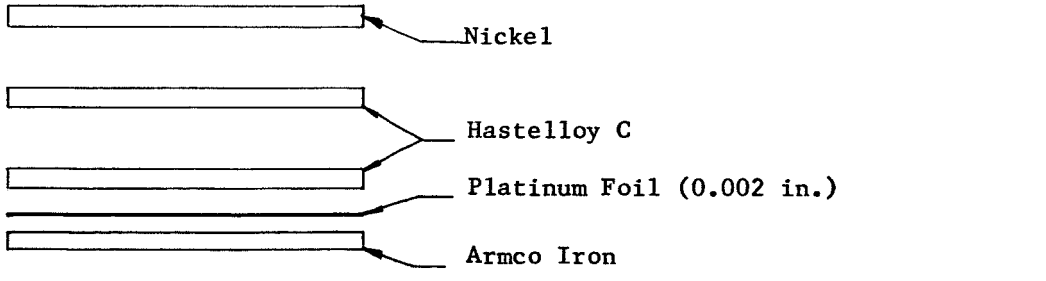

(c) Bonding Coupon Configuration 3
Purpose: Evaluation of Hastelloy C self-bond.
Evaluation of reaction between Hastelloy C and nickel and iron with platinum foil diffusion barrier.

FIGURE 26. EXPERIMENTAL BONDING-COUPON CONFIGURATIONS

Bonding-process parameters: 2100 F, 10,000 psi, 3 hours.

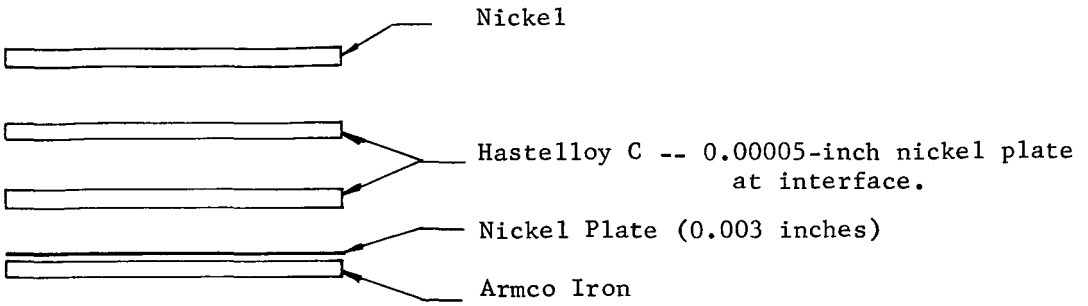

(a) Bonding Coupon Configuration 4
Purpose: Evaluation of Hastelloy C self-bond employing nickel plate as a diffusion aid.
Evaluation of reaction between Hastelloy C and nickel and nickel-plated Armco iron.

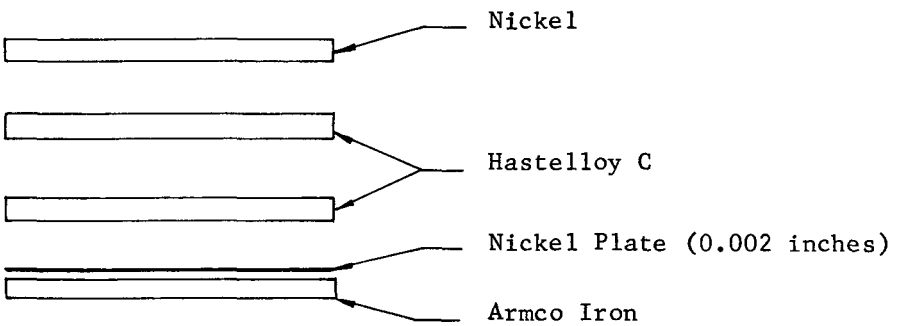

(b) Bonding Coupon Configuration 5
Purpose: Evaluation of Hastelloy C self-bond.
Evaluation of reaction between Hastelloy C and nickel and nickel-plated Armco iron.

FIGURE 26. (CONTINUED)

All components were sealed in a stainless steel envelope by tungsten inert gas (TIG) welding. The final weld closure was made in an electron-beam welder. This was done because the vacuum environment in the weld chamber is retained inside the sealed specimen assembly. Prior to gas-pressure bonding, all sealed specimen envelopes were pressure checked to guard against leaks during the bonding process.

After bonding at 2100 F and 10,000 psi for 3 hours, Configurations 1, 2, and 3 were evaluated by metallographic examination and leaching. The leaching study simply involved leaching the candidate tooling from the Hastelloy C with appropriate acids, which are discussed below, and visually observing the surface of the Hastelloy C that had been next to the tooling.

Metallographic examination of Configuration 1 specimens indicated an extensive diffusion reaction between iron and Hastelloy C, while only moderate reaction was observed between nickel and Hastelloy C (see Figure 27). Intimate contact was realized between the pieces of Hastelloy C but grain growth did not occur across the bond interface. Apparently the nickel plate on the Hastelloy C acted only to inhibit grain growth and not to promote bonding as originally expected. (See self-bond interface in Figure 27.)

Metallographic examination of Configuration 2 specimens revealed a broad reaction zone between the chrome-plated Armco iron and Hastelloy C. Apparently chromium had diffused quite deeply into both components. Only a moderate amount of reaction was observed between the chrome-plated nickel and Hastelloy C, although an intermediate phase had formed between the nickel and Hastelloy C, Figure 28.

The self-bond formed between the Hastelloy C in the Configuration 2 specimen was excellent. No trace of the original interface is evident as grain growth has occurred across the interface along the entire length of the specimen, Figure 28. An additional picture of the bond at higher magnification is shown to illustrate further its excellent appearance, Figure 29.

Examination of Configuration 3 specimens by metallographic techniques indicates that a narrow reaction zone was formed between the platinum and the Hastelloy C on one side and Armco iron on the other, Figure 30. When the composite was leached in hot nitric acid, dissolving the Armco iron and nickel, the platinum-clad surface of the Hastelloy C had a black appearance. Examination of the Hastelloy C self-bond in the specimen revealed a bond which appeared to be of equal quality with the bond in Configuration 2 specimens, Figure 30.

From the results of the first series of specimens described, the following observations were made:

(1) From the extent of diffusion penetration and the appearance of Hastelloy C surfaces after the tooling had been leached, nickel appears to be the most desirable material to have in contact with the Hastelloy C during pressure bonding.

(2) Chrome-plated and platinum-covered nickel and iron tooling left the Hastelloy C surfaces badly discolored after removal of the tooling by acid leaching. It is thought that this condition would result in high emissivity.

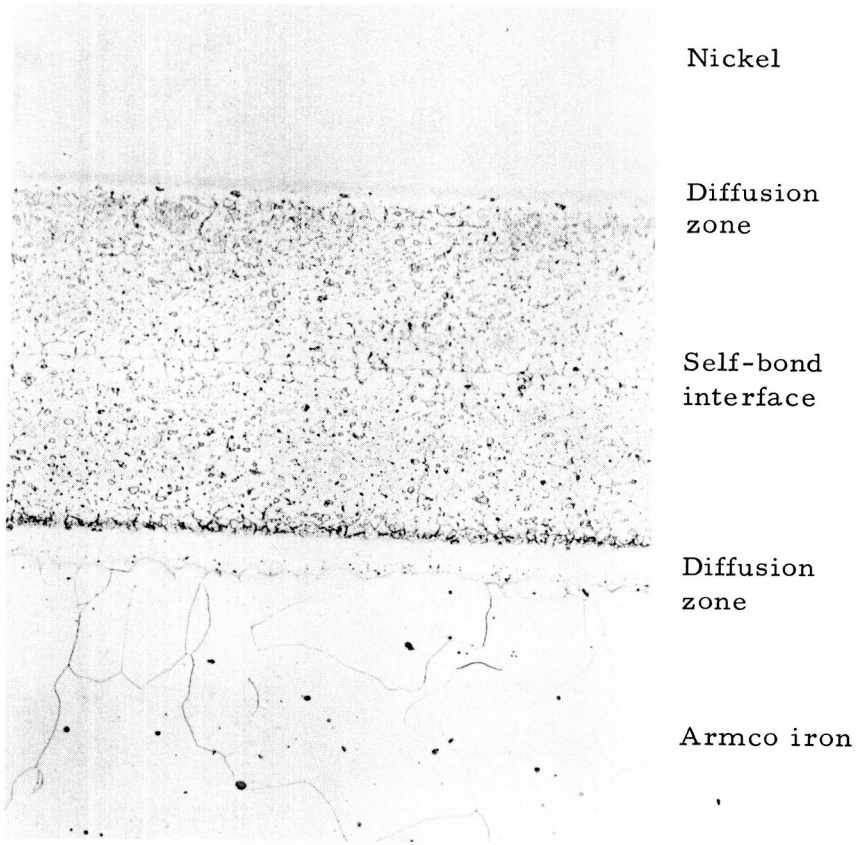

FIGURE 27. METALLOGRAPHIC SECTION OF CONFIGURATION 1 SPECIMEN GAS-PRESSURE BONDED AT 2100 F AND 10,000 PSI FOR 3 HOURS

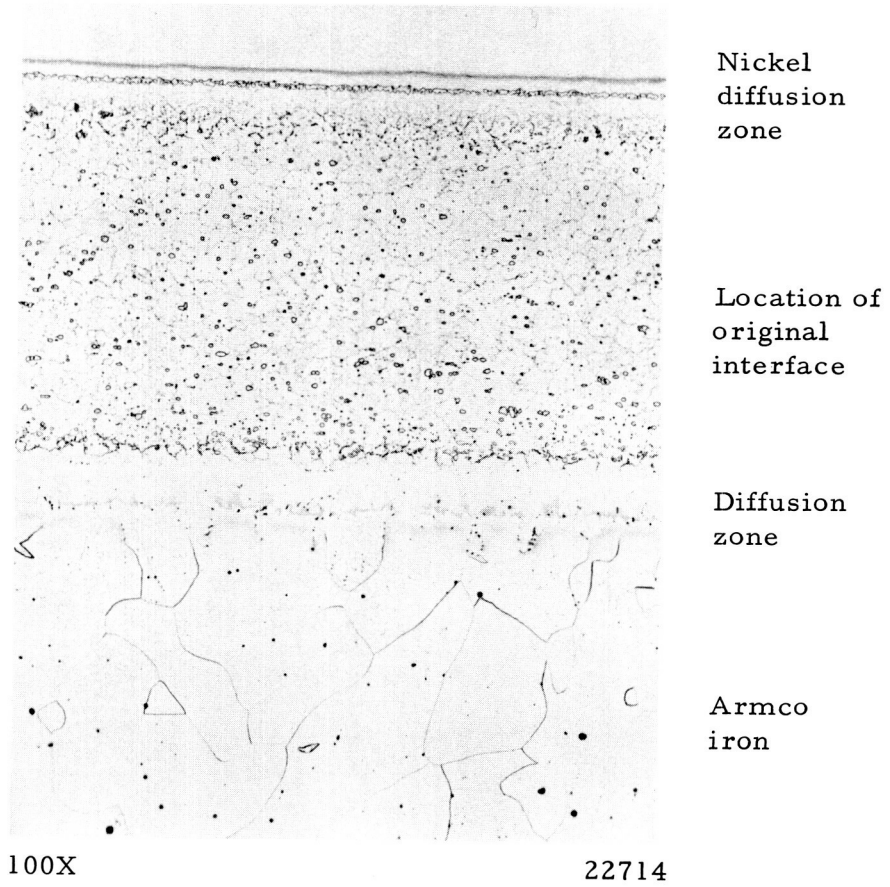

FIGURE 28. METALLOGRAPHIC SECTION OF CONFIGURATION 2 SPECIMEN GAS-PRESSURE BONDED AT 2100 F AND 10,000 PSI FOR 3 HOURS

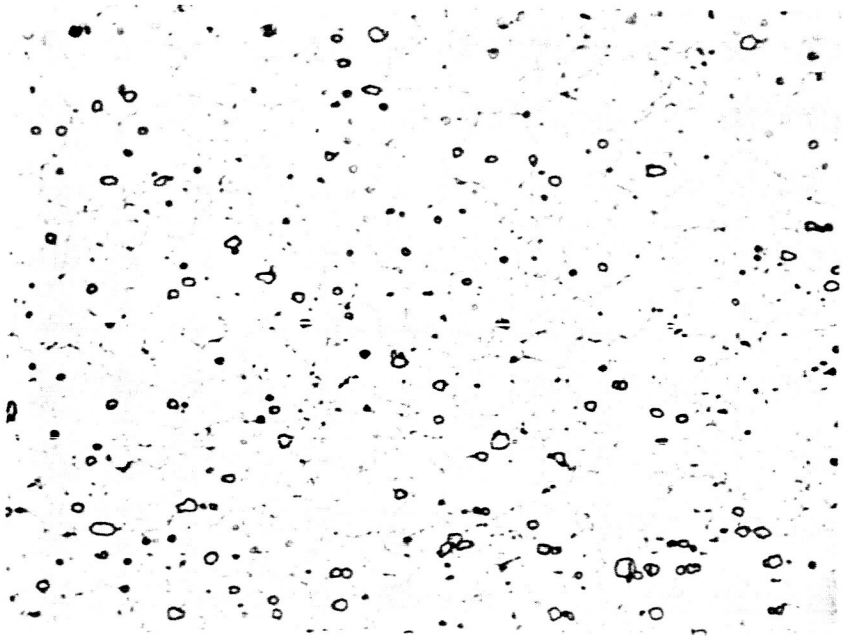

500X 22714B

FIGURE 29. HASTELLOY C SELF-BOND FOUND IN CONFIGURATION 2 SPECIMENS GAS-PRESSURE BONDED AT 2100 F AND 10,000 PSI FOR 3 HOURS

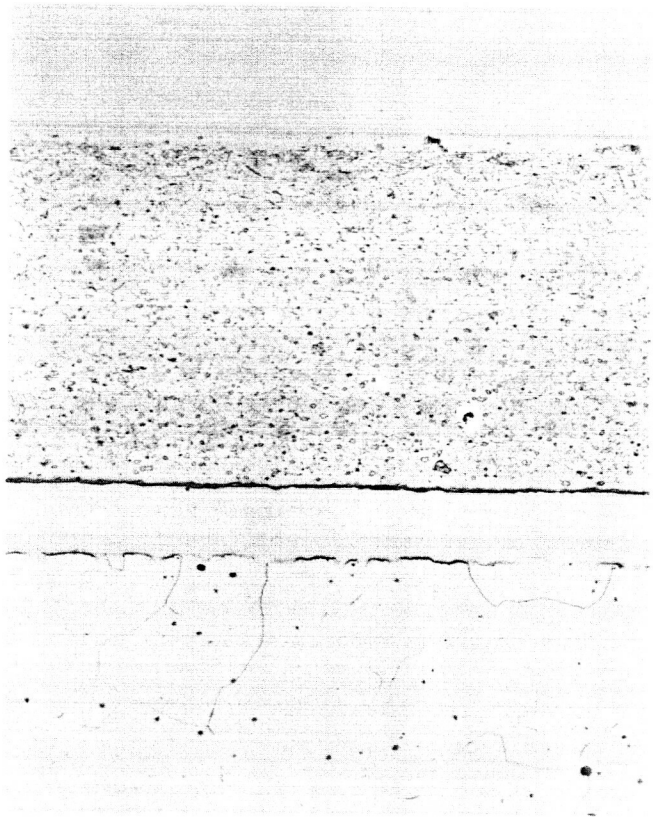

100X 22712

FIGURE 30. METALLOGRAPHIC SECTION OF CONFIGURATION 3 SPECIMEN GAS-PRESSURE BONDED AT 2100 F AND 10,000 PSI FOR 3 HOURS

(3) Sulfuric acid does not dissolve either iron or nickel rapidly enough to be considered for the primary leaching solution.

(4) Hot nitric acid rapidly dissolves Armco iron but attacks the nickel at only a moderate rate.

(5) At temperatures above 190 F, nitric acid rapidly attacks nickel and also attacks Hastelloy C at a potentially destructive rate. Below 180 F, Hastelloy C appears to be completely safe in nitric acid of any concentration.

(6) Excellent Hastelloy C self-bonds were obtained at 2100 F and 10,000 psi for 3 hours.

Regarding the last conclusion, the bond zones appear largely the same as the base material and, therefore, should have similar strength. It is believed that the elevated-temperature exposure followed by slow cooling will not alter the properties of the as-received sheet. Though noticeable precipitation is present, Figures 28, 29, and 30, it is the opinion of the research staff at Union Carbide's Stellite Division* that there will be no significant effect on either the thermal or mechanical properties when Hastelloy C is slow cooled from the 1800 F to 2100 F temperature range. Several Hastelloy coupons were acid soaked to determine whether the acid-corrosion-resistance properties of the alloy were retained. After many hours of soaking, no attack was observed, indicating to some extent that the as-received properties were maintained through the bonding process. Strength properties will be verified with tensile specimens of the alloy before and after bonding.

Improvement of Surface Finish. An attempt was made to improve the surface finish of Hastelloy C that had been in contact with nickel during the 2100 F bonding cycle. Specimens were immersed in a slurry of silicon carbide grit and water. The specimens were held stationary while the slurry was vibrated, first at a high frequency and low amplitude, and then at a high amplitude and low frequency. Microscopic examination of the metal surfaces was made at various time intervals during each vibratory exposure. Little or no improvement in surface finish was noted for total polishing times of up to 12 hours. Surface polishing using ultrasonic and low-frequency vibratory techniques does not appear to improve the surface finish of Hastelloy C.

In an effort to decrease the diffusion interaction between Hastelloy C and the tooling, and possibly improve the final surface finish, additional specimens of Configurations 4 and 5, shown in Figure 27, were prepared and bonded at 2000 F instead of at 2100 F. The specimens consisted of 1-1/2-inch-square coupons. The two specimens were assembled and sealed in a stainless steel envelope for gas-pressure bonding. Bonding was done at 2000 F and 10,000 psi for 3 hours.

After bonding, the specimen configurations were sectioned and examined metallographically. The Configuration 4 specimen did not exhibit grain growth across the self-bond interface, Figure 31. This was also observed in the Configuration 1 specimen bonded at 2100 F. In both instances, the nickel plate acted to inhibit rather than promote bonding. In the Configuration 5 specimen, grain growth had occurred across the self-bond interface, leaving little or no evidence of the original interface, especially when viewed at high magnification, Figure 32. Some shading discontinuity occurred at

*Personal communication with C. L. Barkin.

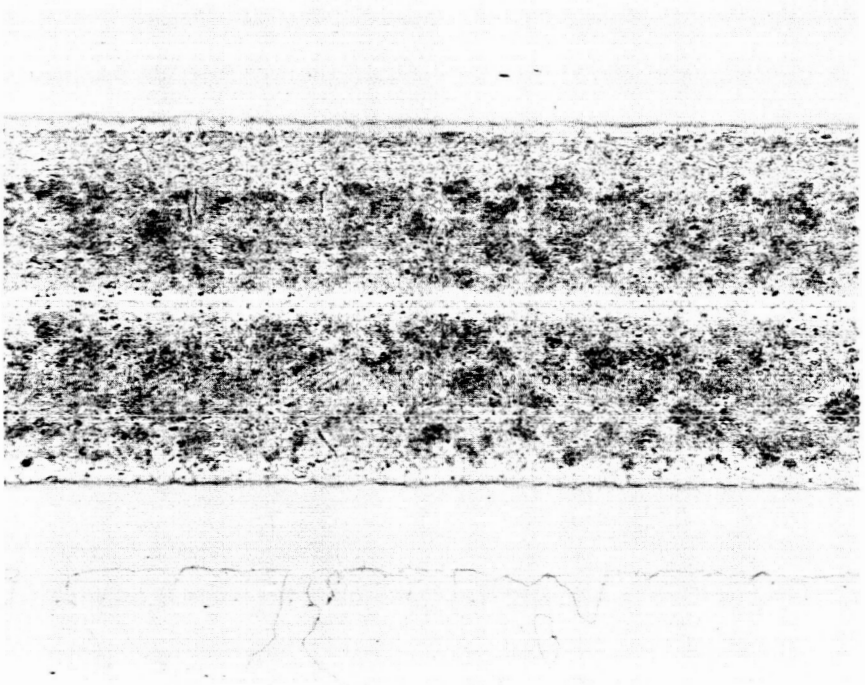

100X 23294

FIGURE 31. METALLOGRAPHIC SECTION OF CONFIGURATION 4 SPECIMEN GAS-PRESSURE BONDED AT 2000 F AND 10,000 PSI FOR 3 HOURS

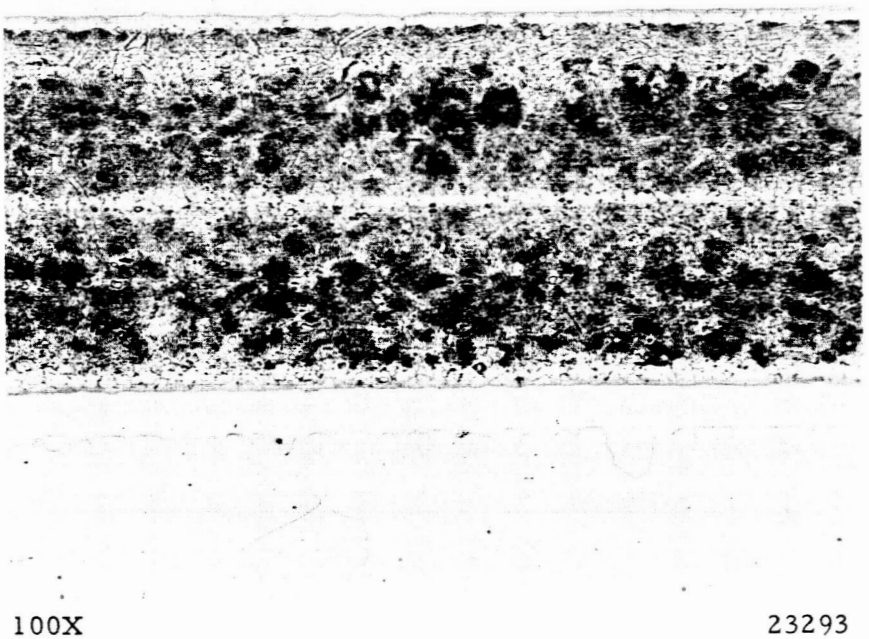

100X 23293

FIGURE 32. METALLOGRAPHIC SECTION OF CONFIGURATION 5 SPECIMEN GAS-PRESSURE BONDED AT 2000 F AND 10,000 PSI FOR 3 HOURS

the interface, but this is due to the degree of second-phase precipitation across the specimen. Second-phase precipitation is less at the original Hastelloy C alloy surfaces, probably because of alloy depletion from heating operations during the production of the sheet stock. As expected, diffusion reaction between the Hastelloy C, nickel, and the nickel-plated Armco iron was considerably less than observed when bonding was performed at 2100 F.

The composite nickel-plated-iron and solid-nickel tooling was removed by leaching in hot nitric acid. The composite tooling was dissolved as readily as plain iron tooling, and much more rapidly than solid nickel. The surface of the Hastelloy C that had been in contact with the tooling had a metallic luster, and visually appeared considerably improved over the surfaces obtained from the specimens bonded at 2100 F. The 0.003-inch-plate thickness appeared to give better results than the 0.002-inch thickness of nickel plate on the Armco iron. Although both platings gave good results, the Hastelloy surfaces bonded against solid nickel appeared to be the most reflective.

A subsequent surface-finish evaluation was conducted by making an emittance measurement on the most promising of the coupons bonded at 2000 F. This coupon (Configuration 4, Figure 26) was bonded with one face against solid nickel and the other face against Armco iron plated with 3 mils of nickel. Visibly, the latter side was slightly less reflective after leaching. Thus, the emittance measured is probably slightly higher than that which may be achieved with solid-nickel tooling. The measured values for the emittance are shown below:

Temperature, C	Hemispherical Total Emittance
229.0	0.18
252.9	0.18

This emittance value lies between the values given in the literature[4] for polished and shot-blasted nickel; thus, the surface-finish evaluation was concluded.

Selection of Optimized Bonding Process. On the basis of the results described above, the bonding temperature was established as 2000 F. Nickel-plated Armco iron was chosen for the filler tooling. Since, as mentioned previously, solid-nickel tooling, although giving the best surface appearance, would be too difficult to remove from the structure, 2-1/2 mils of nickel plate on Armco iron was selected as being the minimum thickness of nickel which would produce the desired surface finish and still allow rapid removal of the tooling. Nitric acid was chosen as the tooling leachant.

Component Fabrication

This effort includes fabrication of the insulation foils, webs, end plates, and filler tooling. The filler tooling, discussed above, is required to effect internal spacing of the structures during bonding. After bonding and machining of the specimens, the filler tooling will be removed from the structures by selective acid leaching. Web and filler

(4) Wood, W. C., Deem, H. W., and Lucks, C. F., DMIC Report 177, Vols 1 and 2, November 15, 1962.

piece configurations require each layer of the Series 1 structures to have seven filler pieces, and those of Series 2 to have 11 filler pieces. Because of the varying web thicknesses, the tooling pieces had to be custom designed to assure symmetric web intersections in adjacent layers. Four types of filler pieces are required. These are shown in Figure 33, a and b.

The filler tooling was machined from 0.095-inch Armco iron blanks which were sheared from rolled sheet. More than 1000 pieces made were processed in bound groups of 50 and 35 pieces. The machined filler pieces were then plated on all sides with 0.0025 inch of sulfate nickel, as required by the bonding process.

Prior to fabrication of the structural webs, investigations were carried out to determine the simplest web-generation method. Web-corrugation experiments were carried out using an available die which was designed to form webs with a 0.3-inch web-bend length from 10-mil stainless steel stock. Sample webs were formed with this same die from 5-mil, 10-mil, and annealed 10-mil Hastelloy C stock. The webs thus formed were compared with each other, with the previously formed stainless steel webs, and with an available piece of filler tooling to note differences in springback, straightness, and fit to the piece of tooling. It was determined from these observations that webs of different thickness (4 mil, 8 mil, and 12 mil) may be corrugated with one die for each of the two proposed web-bend lengths. Thus, two web-corrugating dies were designed. The die surfaces were 4340 steel. The dies are shown in Figure 34, a and b.

The webs were sheared from annealed Hastelloy C foil and corrugated using the dies in an automatic press. Subsequent to corrugation, the webs were stacked together to be ground to the proper height, 0.052 inch, which is 2 mils greater than the plated tooling height to allow for some upset in the bonding process. In the assembly process, the webs were snipped to the proper length. Corrugated webs may be seen in Figure 34.

Material for the foils was received in strip form and was only required to be sheared into 3-1/2-inch squares. The thicker end pieces required machining of the edges to assure proper fit in the assembly frames. These pieces of the assembly are discussed and shown in the following section.

Assembly and Bonding

One of the basic steps in the process of producing the required insulation specimens is the cleaning and assembly operation. It is extremely important if reproducibility is to be expected.

The corrugated webs, foils, plated tooling, and can components were separated into appropriate groups and cleaned in preparation for assembly and bonding. All Hastelloy C components were cleaned by degreasing in methyl-ethyl-ketone, pickled in acid for 2 to 5 minutes, rinsed in distilled water, dipped in ethyl alcohol, and dried under a heat lamp in a dust-free area. The acid solution consisted of 50 parts concentrated nitric acid, 10 parts concentrated hydrofluoric acid, and 40 parts distilled water.

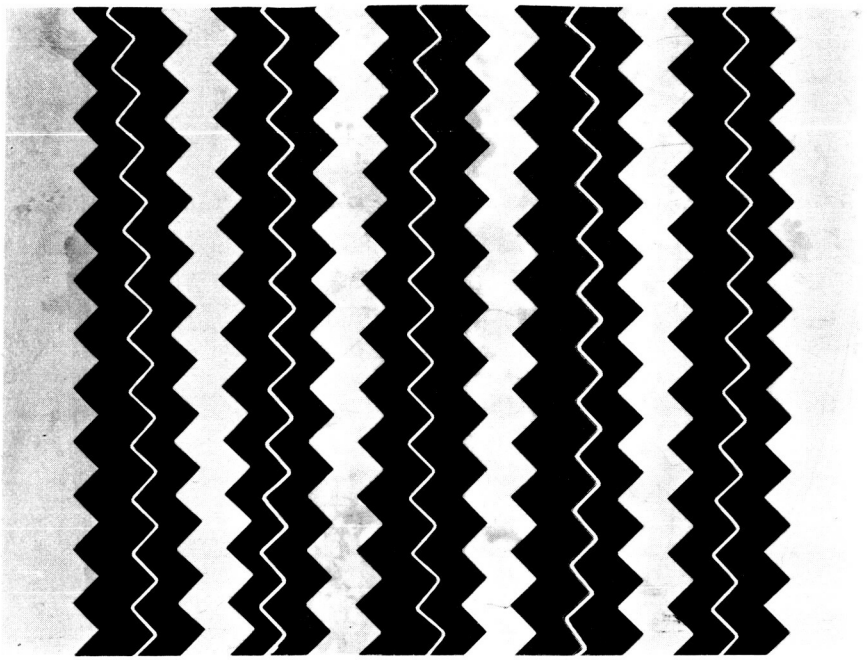

25920

a. 1/2-Centimeter Web-Bend Length

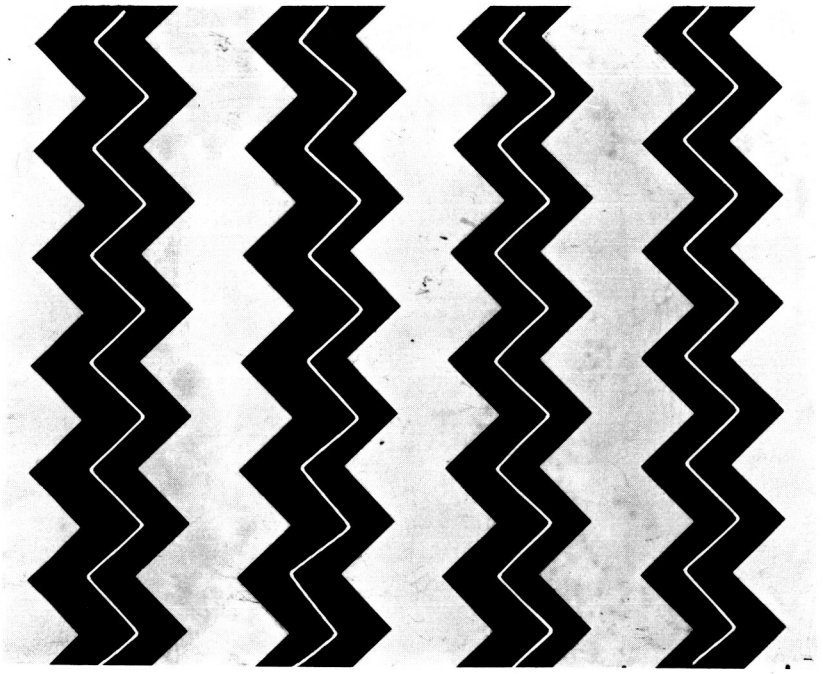

25919

b. 1-Centimeter Web-Bend Length

FIGURE 33. TYPES OF FILLER TOOLING PIECES SHOWING TWO WEB-BEND LENGTHS

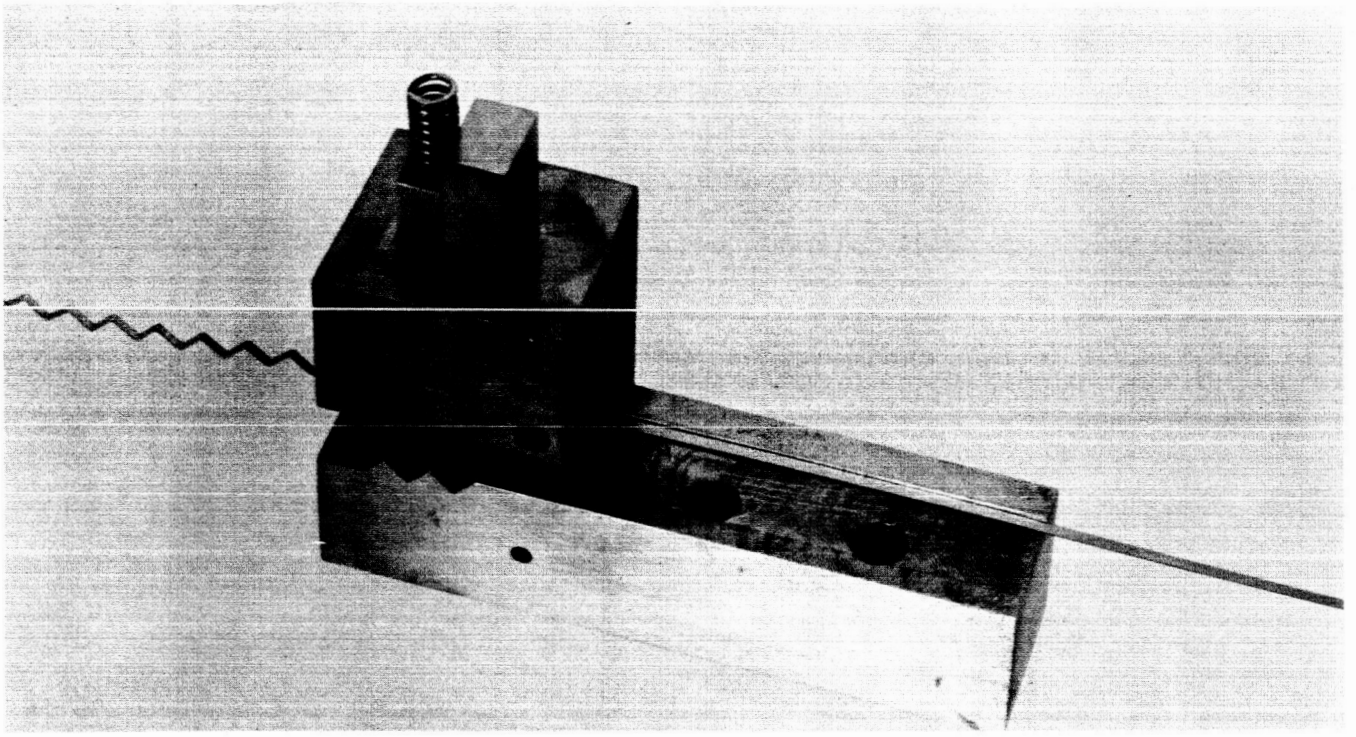

a. 1/2-Centimeter Web-Bend Length 25917

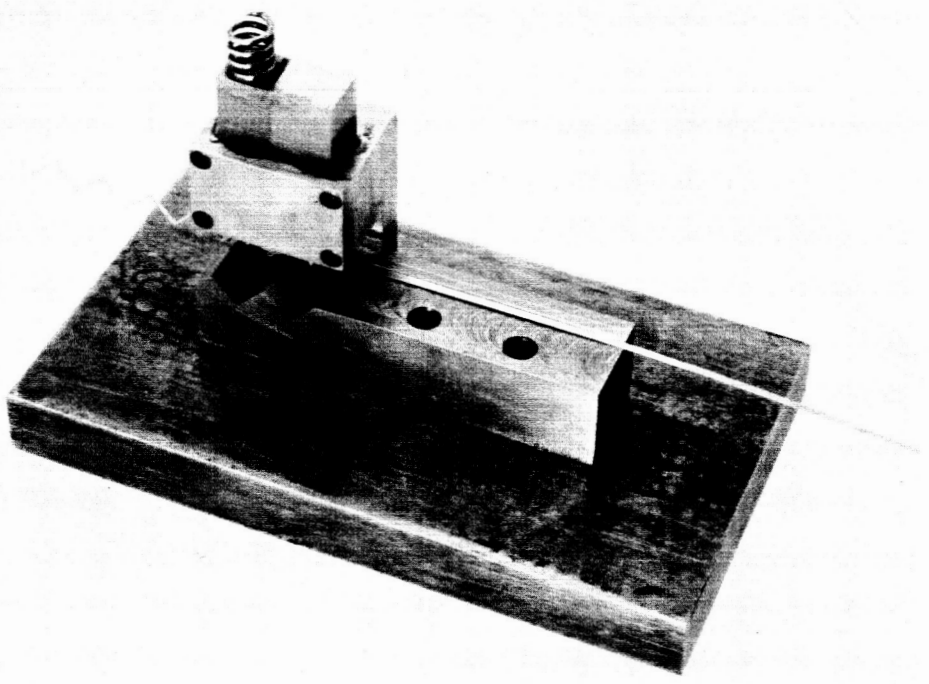

b. 1-Centimeter Web-Bend Length 25918

FIGURE 34. WEB-CORRUGATION DIES

The nickel-plated tooling and steel-can components were cleaned in a strong alkaline solution, rinsed in distilled water, dipped in ethyl alcohol, and dried under a heat lamp in a dust-free area.

After cleaning, each group of components was placed in labeled polyethylene trays with tight-fitting lids to retain them in the as-cleaned condition.

The trays containing the components were taken to a special air-conditioned room for assembly. The assembly room, although not an actual "clean room", had been thoroughly scrubbed before the components for assembly were brought into the area. The air in the room was filtered and maintained at a constant 68 degrees, and access was provided only to those people connected with the assembly process. White cotton gloves and degreased tools were used by the personnel doing the assembly and handling. Figure 35 is a view of the assembly table.

The specimens were assembled by placing the appropriate components into prefabricated "picture-frame" cans. Figure 36 shows the picture-frame can on the right and the other components, going from left to right, in the order in which they are placed in the can.

After the components were placed in the picture frame, a stainless steel cover plate was welded in place. The can was then final sealed by electron-beam welding, retaining the vacuum inside the sealed envelope. Before loading into the autoclave, the specimens were all leak checked. The 18 assembled specimens were gas-pressure bonded in two groups of ten each at 2000 F and 10,000 psi for 3 hours. From visual inspection, all specimens appeared to have "pressed" during the bonding cycle, as verified by postbonding leak checks.

After bonding, the specimens will be machined to proper size for the thermal and structural tests, which will be performed during the next work period, and the tooling will be leached from the structures with acid.

Summary

Satisfactory self-bonding of Hastelloy C can be achieved at 2000 F and 10,000 psi for 3 hours. Use of the lower bonding temperature appears to result in a significant improvement, over initial runs at 2100 F, in surface finish of the Hastelloy C after leaching of the composite tooling. A sulfate-nickel plate, 0.0025 inch thick, on the Armco iron tooling has been determined to be satisfactory in preventing diffusion of the iron into the Hastelloy C while at the same time affecting efficient leaching of the composite tooling with nitric acid.

The insulation components have been assembled into structures. Each structure has been separately sealed in an evacuated can and subjected to the autoclave bonding process.

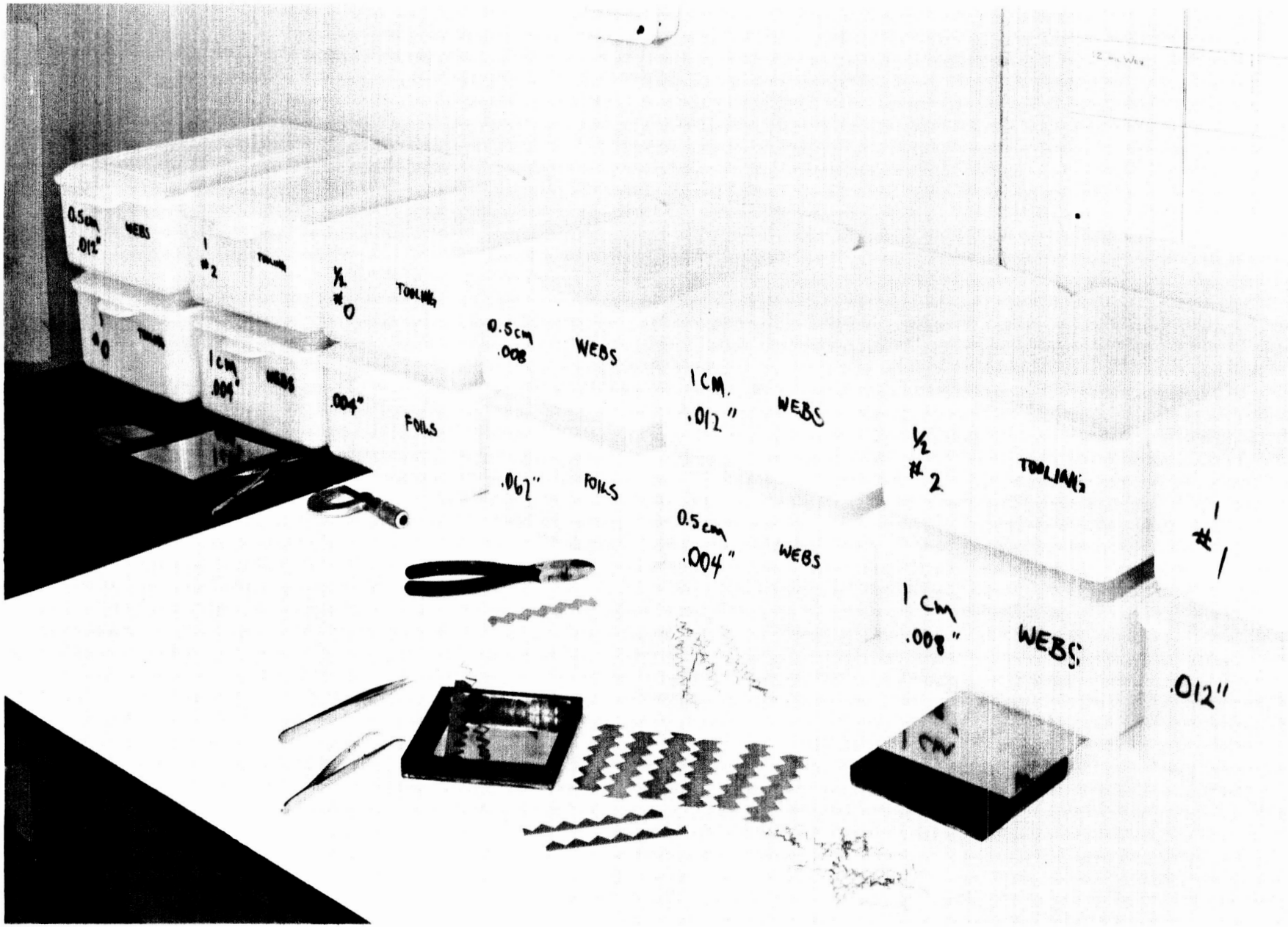

FIGURE 35. ASSEMBLY AREA SHOWING COMPONENTS STORED IN POLYETHYLENE TRAYS WITH TOOLS AND COMPONENTS IN FOREGROUND

25915

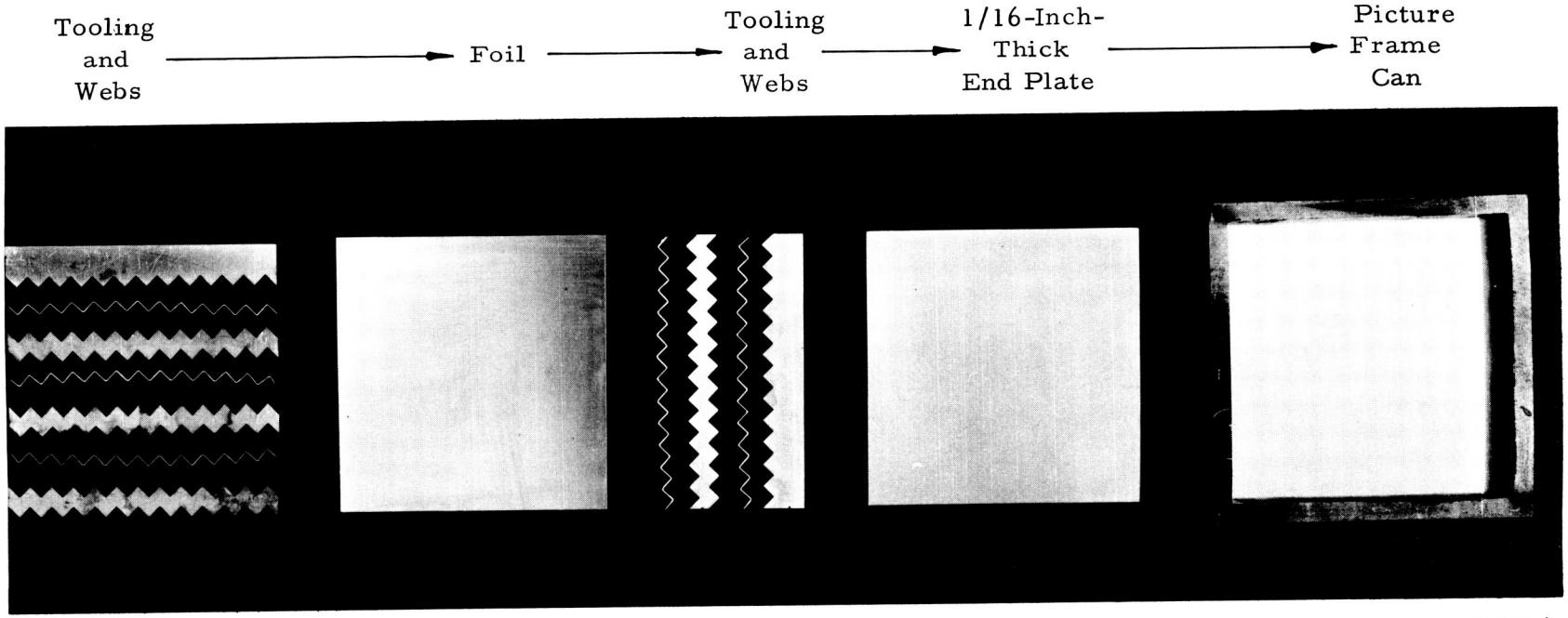

FIGURE 36. PICTURE-FRAME CAN AND INSULATION COMPONENTS IN THE SEQUENCE OF ASSEMBLY